Abandonment of solution mining cavern field Zuidwending, The Netherlands

Statement on Hydraulic Fracturing Risk

– an integrated, multiscale investigation –

06 February 2025

by

CCC

Cavern Closure Consortium

Brouard Consulting SAS	5.1.2.e [redacted]
MaP - Microstructure and Pores GmbH	5.1.2.e [redacted]
smartTectonics GmbH	5.1.2.e [redacted]

* Responsible author

Cavern Closure Consortium · MaP Microstructure and Pores GmbH · BROUARD CONSULTING · smart Tectonics GmbH

Content

Disclaimer

This report has been prepared by the Cavern Closure Consortium (CCC), an independent research consortium commissioned by Nobian Industrial Chemicals to conduct an integrated, multiscale investigation into the abandonment of the Zuidwending solution mining cavern field in the Netherlands. The present document is based on findings presented in the final report of the respective abandonment study (Abandonment of solution mining cavern field Zuidwending, The Netherlands – an integrated, multiscale investigation, version 240411) and reflects the current state of knowledge, incorporating relevant research aspects as well as insights from Nobian's operational activities.

The primary objective of this report is to provide further explanations and visualizations based on the final report (Abandonment of solution mining cavern field Zuidwending, The Netherlands – an integrated, multiscale investigation, version 240411).

This report should not be regarded as a legally binding document. Neither CCC nor its members shall be held liable for any decisions or actions taken based on the information contained herein.

NOMENCLATURE

Latin symbols

SYMBOL	DESCRIPTION	UNITS
FBP	Formation breakdown pressure	bar
FOS	Factor of Safety for the onset of dilation	–
g	Gravity acceleration	m/s²
I_1	First invariant of the stress tensor	MPa
J_2	Second invariant of the stress tensor	MPa²
LOP	Leak-off pressure	bar
LOT	Leak-off test	–
P_c	Cavern pressure	bar
P_f	Pore pressure	bar
P_{over}	Hydrostatic pressure in the overburden	bar
T_0	Tensile strength of salt	MPa
t	Time	day
v	Brine velocity through a fracture	m/s
Z_{cav}	Depth of the top of a cavern	m
Z_{over}	Depth of the base of the overburden for a cavern	m
z	Depth	m

Greek symbols

SYMBOL	DESCRIPTION	UNITS
α	Biot's coefficient	–
βV	Cavern compressibility	m³/bar
Δp	Fluid pressure minus least compressive principal stress	MPa
ΔZ	Thickness of salt roof	m
ρ	Rock density	kg/m³
ρ_b	Saturated brine density	kg/m³
$\rho_{\max}$	Maximum pressure gradient reached at the cavern roof of a cavern during computations	bar/m
ρ_w	Water density	kg/m³
σ_1	Most compressive principal stress	MPa
σ_2	Intermediate principal stress	MPa
σ_3	Least compressive principal stress	MPa
σ_{geo}	Geostatic stress, stress exerted by the weight of overlying rock strata	MPa
σ_{oct}	Octahedral shear stress	MPa
σ_H	Most compressive horizontal stress	MPa
σ_h	Least compressive horizontal stress	MPa
σ_V	Vertical stress	MPa

1 Executive Summary

The questions

This document, based on the CCC's work, aims to answer a number of questions concerning the risk of hydraulic fracturing and, more generally, the long-term stability of the Zuidwending caverns. The main questions are as follows:

- Is there a risk of the caverns collapsing and creating a sinkhole on the surface?
- Can we rule out the risk of fractures appearing in the cavern walls after abandonment?
- If fractures do occur, what could be the consequences?
- What is the difference between likelihood and effect of hydraulic fracturing between end of mining in 2025 compared to the planned end situation?

The methodology

In the CCC report submitted to Nobian and Gasunie in April 2024, the behaviour of the salt production and storage caverns was modelled in both 2D and 3D, utilizing all available information and making use of the latest scientific advancements. As a result, this approach can be considered the state of the art in this field. The analysis considered the entire history of the caverns, divided into three key phases: the mining period, a waiting period prior to abandonment, and the post-abandonment period extending up to the year 2250.

Since April 2024, the models have been improved, in particular with regard to the creep parameters of the different salt facies and also with a better estimate of salt porosity. The results of the calculations with these improvements are used in this document to answer the questions stated above.

The main findings

- ✓ The creation of a sinkhole is extremely unlikely (estimated in the order of magnitude of lower than 10^{-6}) for all caverns in Zuidwending because, in the realistic estimates, they are more than a hundred metres (minimum distance where stability has been proven) from the sides of the dome. Furthermore, the caverns are relatively deep with a very thick salt roof, significantly distancing them from the overburden.

- ✓ The numerical simulations demonstrated that, even under very conservative assumptions, the caverns maintain mechanical stability over the long term, although the risk of minor hydraulic fractures in close proximity to the salt caverns (< 15 m) cannot be completely ruled out. The likelihood of massive sub vertically propagating hydraulic fractures is considered very unlikely as the simulation do not indicate dilation or favourable stress conditions for this to happen.

- ✓ Since the report’s submission in April 2024, additional insights have emerged from discussions and updated simulations. While these new findings have not altered our overall interpretation of the caverns’ long-term stability, they do provide opportunities to refine our understanding of key aspects. These refinements specifically relate to dilation, the likelihood of sinkhole formation, and the potential occurrence of hydraulic fractures.

- ✓ Before abandonment, pressure decreases to halmostatic conditions may cause some damage in the first few meters around the cavern wall, leading to localized dilation and permeation. However, the likelihood of hydraulic fractures propagating beyond 15 meters remains negligible.

- ✓ After abandonment, permeation is expected, particularly near the cavern wall and roof. In the first months to years following abandonment, when pressure increases at a relatively high rate, small-scale hydraulic fracturing could also occur in these areas. Nevertheless, the propagation of hydraulic fractures beyond 15 meters remains highly unlikely.

- ✓ In the long term, as stress differences decrease and brine warming decreases, permeation may continue, but the likelihood of hydraulic fracture formation diminishes further. While hydraulic fractures cannot be completely ruled out, the possibility of a large subvertical fracture propagating beyond 15 meters from the cavern wall is extremely low.

- ✓ In the case of stopping mining at the end of 2025, the likelihood of hydraulic fracturing is comparable to or even slightly higher than the planned end situation. The volume that could leave the cavern will be ~25% lower in the case of stopping mining in 2025, meaning a worst case maximum of ~6500 m^3. The calculated outflows in the hydraulic fracturing chapter are based on the planned end situation.

- ✓ After considering several scenarios and the planned end volume of a representative cavern, it appears that the volume of brine that could escape from the cavern to surrounding layers through one of several fractures remains very limited, ranging from 540 m^3 to 8,600 m^3.

2 Assessment of the Likelihood of Sinkhole Formation

2.1 Short summary

The probability of the formation of a sinkhole in Zuidwending is negligible (i.e. estimated to be smaller than 10^{-6}[*]) and can realistically be ruled out during the entire lifecycle of the caverns, including the abandonment phase. Given the configuration of the Zuidwending cavern field, no realistic process is imaginable that could lead to the formation of a sinkhole. Firstly, because the caverns are sufficiently far away from the edges of the dome and the overburden. Secondly, the numerical calculations carried out have shown that the pillars between caverns remain very stable in the long term, with no overloading or significant dilation that could jeopardise their stability. These conclusions are presented in more detail below.

[*] According to Nobian document 12.01.6.OP11 Hazard Studies (page 18, figure 8). A key principle in the approach to risk assessment is that the rigor of the risk assessment methodology should be proportionate to the complexity of the problem and the magnitude of the hazard and the risk. Therefore these type of risks (based on an estimated combination of frequency/likelihood and severity) may be estimated qualitatively in orders of magnitude.

2.2 Configuration requirements for creating of a sinkhole

The different configurations that can lead to the formation of a sinkhole above a cavern field are described in Karimi-Jafari et al. (2008) and Bérest et al. (2016, 2017). We can briefly summarise the conclusions of these articles:

- Sinkhole formation occurs almost exclusively in shallow caverns. It is difficult to define precisely what constitutes a shallow cavern, but the limit is generally set at less than 500 m deep (Bérest, 2017; CCC, 2019).

- Three mechanisms can be distinguished: first, in most cases, at the end of mining, the cavern roof had reached the top of the salt formation, allowing direct contact between brine and marl (or argillite) layers that compose the overburden of the salt formation. These layers can collapse layer for layer into the cavern. Secondly, a piston-type collapse, with a sinkhole with initially vertical walls, can occur when a rigid cylinder of salt falls into the cavern. A third, hourglass-type mechanism occurs when a cavern moves upwards through the stratigraphy, until the uppermost bedrock at shallow depth is breached, permitting loose materials to flow into the cavern through a relatively narrow hole at the bottom of the sinkhole, as in an hourglass.

- In the vast majority of cases, the issue is attributable to the presence of a roof or wall of salt that is too thin, with a thickness of less than a few metres, between the cavern and the non-salt rock.

These sinkhole-creating mechanisms cannot occur at Zuidwending, as the caverns are relatively deep and sufficiently remote from other formations (more than 100 meters based on realistic interpretations).

2.3 Case histories for deep caverns

In the literature, we know of only one example of a relatively deep cavern (the roof is at a depth of 1040 m) that collapsed, creating a sinkhole on the surface, namely the Bayou Corne sinkhole in Louisiana (Bérest, 2017; Bérest et al., 2020). This is a very special cavern, located very close to the flanks of the salt dome (Figure 1), even if the exact minimum distance, likely less than 30 m and surely much less than 100 m, has not been determined very precisely. The breach in the salt wall is likely to have occurred in the lower part of the cavern, where the salt-wall thickness was minimal. When this cavern was abandoned with no waiting period, brine pressure at cavern top built up to a level such that the loss of volume was balanced by the loss of brine at the bottom of the cavern flowing downward through the sediments. Sediments flowed from the sideburden to the cavern as a highly viscous material through a Disturbed Rock Zone (DRZ) along the dome edge. However, this flow through the U-Tube was not frictionless as occasional "stick-and-slip" phenomena occurred. This incident was linked to a particular context and a lack of caution. The location of the sides of the dome was not well known and the cavern turned out to be much too close to the sides. Furthermore, no serious abandonment study had been carried out prior to the abandonment. More information can be found here: https://www.dnr.louisiana.gov/.

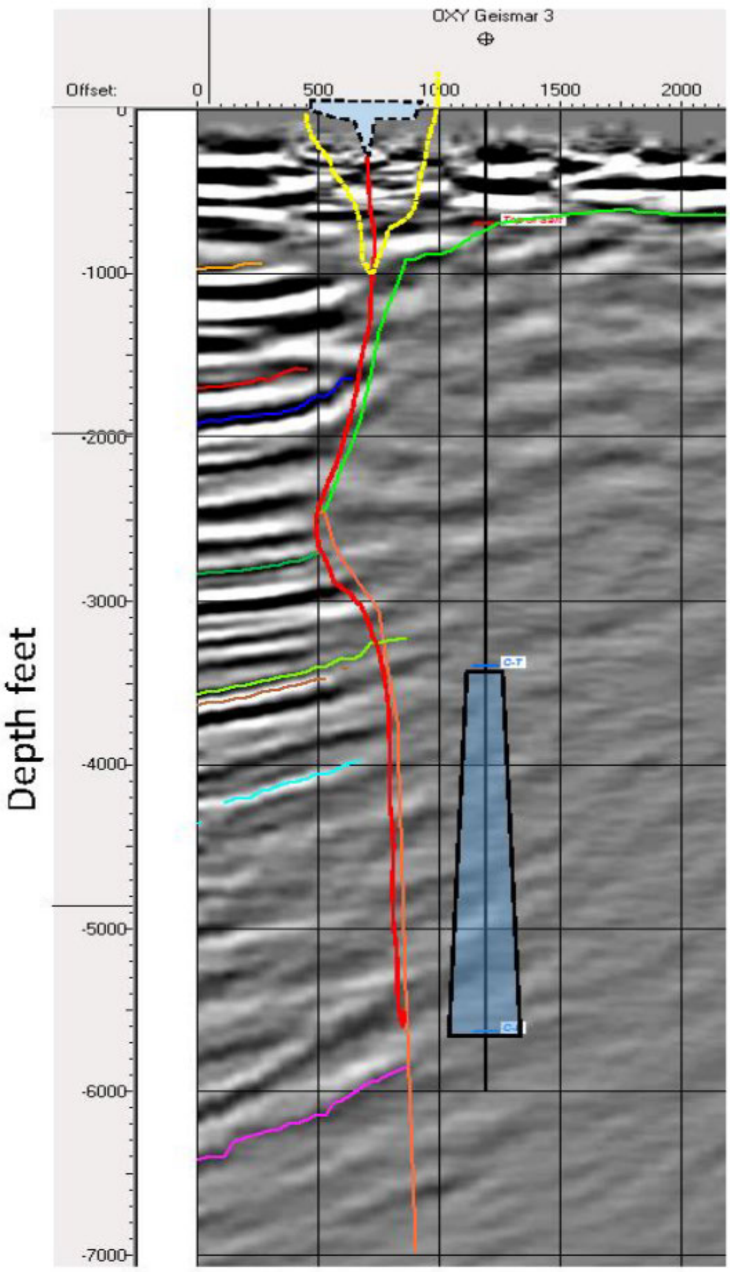

Figure 1. The Oxy3 cavern and the flank of the dome (Bérest, 2016).

In recent years, concerns have arisen regarding the potential formation of a sinkhole at another site in Louisiana, the Sulphur Mines dome. Detailed information on this event can be found on the website of the Louisiana administration in charge of these problems (https://www.dnr.louisiana.gov/page/sm-1homepage). This configuration is relatively similar to that of the Bayou Corne cavern, but unlike the Bayou Corne cavern, the Sulphur Mines cavern was still being used for brine production when the leak occurred. In this case no sinkhole has yet formed, although it is thought that it may do so in the future. Analyses have shown that this cavern is very close to the side of the dome, although it is difficult to give a precise distance, likely much less than 100 m. A major brine leak occurred during leaching operation at the end of 2021, forcing the operator to pump brine continuously at a very high rate (currently larger than 2 m^3/min) to maintain the pressure in the cavern. To date, 1.5 million m^3 of brine have been injected into this cavern, which has a volume of 1.6 million m^3. These figures show that a hydraulic connection was established between the cavern and highly permeable layers, probably with depleted gas, outside the salt dome. To explain the creation of the connection, the geomechanical analyses currently underway suggest the presence of a relatively weak salt between the cavern and the sides of the dome. A dam is currently under construction to contain the damage on the surface should a sinkhole form.

The situation at the cavern field in Zuidwending is not comparable to that at the Bayou Corne and Sulphur Mines. The field was designed with a minimum salt thickness of 200 metres between the caverns and both the top salt and the dome flank. Only one cavern does not fully comply with this design, ZW-1, which has a minimum distance of 139 metres (± 40 metres) to the salt dome flank (Figure 2 and Figure 3). This cavern is no longer producing and Nobian plans to conduct a field test with partial backfilling to ensure safe abandonment. In contrast to the situation at the Louisiana Sulphur Mines, there were no irregularities during operation or standstill in Zuidwending.

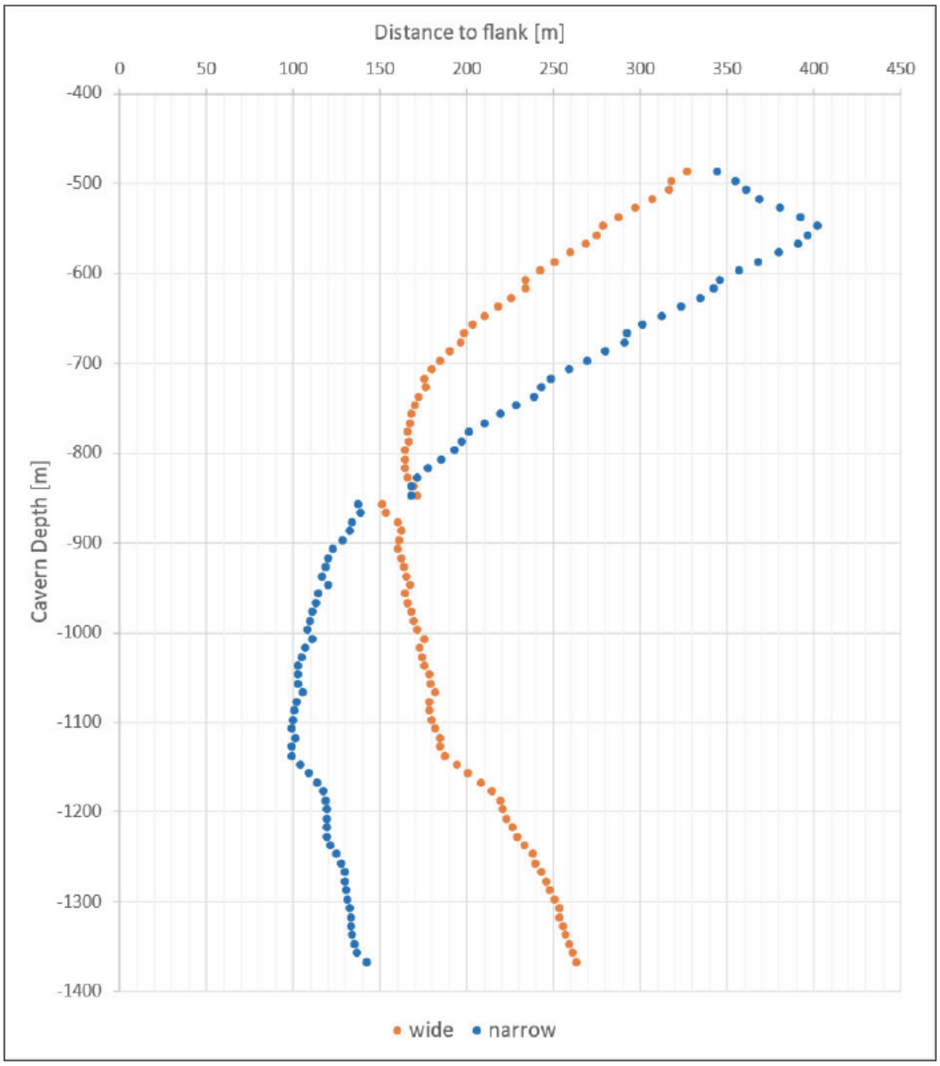

Figure 2. Distance of cavern ZW-1 to flank.

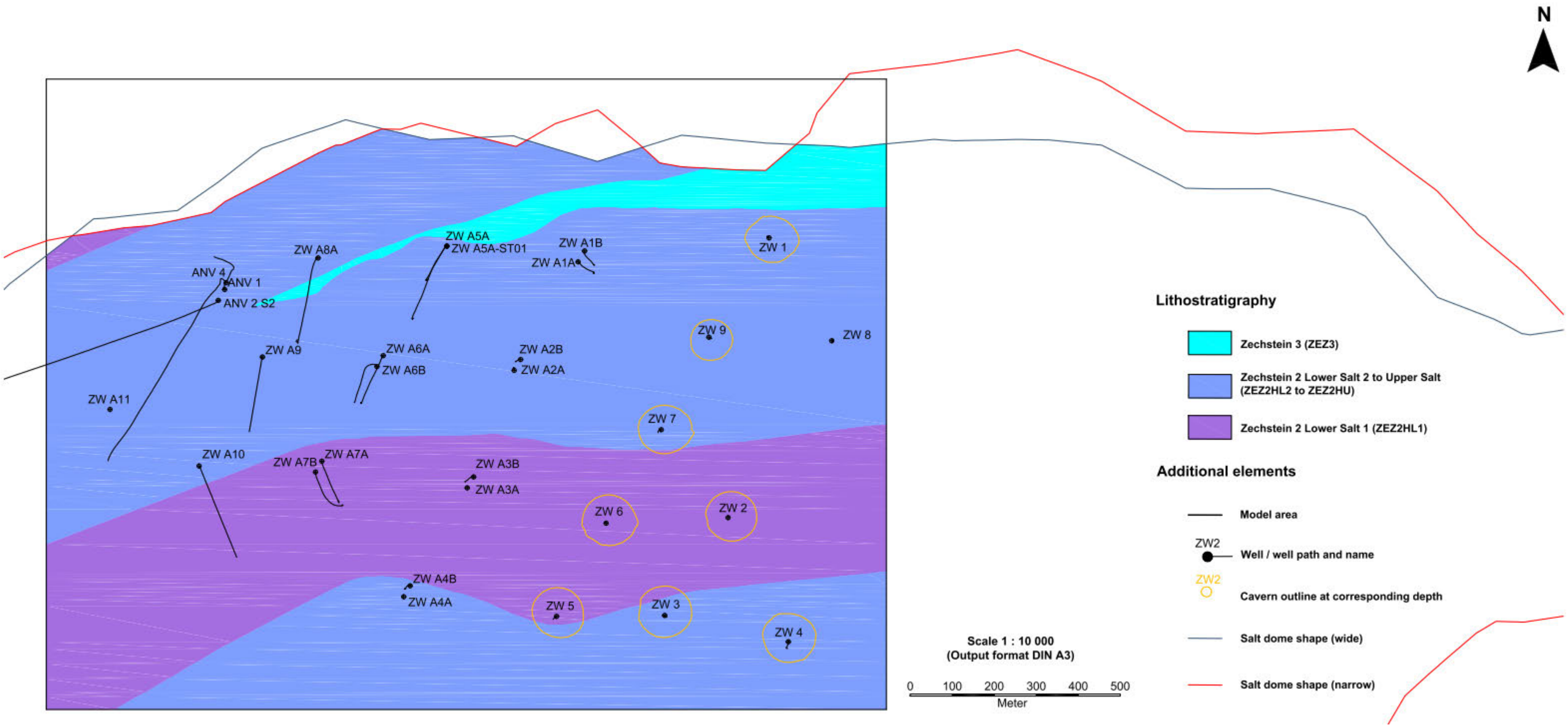

Figure 3. Horizontal sections at a 1000-m depth for the Zuidwending salt dome (DEEP.KBB, 2020).

2.4 Onset of dilation

An increase in salt volume can occur under certain compressive stress states. This volume increase is due to salt micro-fracturing, a phenomenon called dilation. Salt dilation must be avoided during operations, as it may cause an increase in salt permeability, and probably also an increase in porosity and storativity, and a reduction in salt strength. Several dilation criteria can be found in the literature. If the core of the pillars between the caverns were to dilate, as well as the salt roof between the caverns and the top of the salt dome, there would be a risk of collapse, as happened in the Varangéville salt mine in 1873 (Bérest et al, 2008). According to the various numerical simulations carried out by both Brouard Consulting and smartTectonics, there is no risk of collapse due to dilation in Zuidwending.

The computations consider two very conservative hypotheses regarding the onset of dilation:

- We considered the RD criterion (DeVries, 2006), which has the advantage of being conservative, as it takes into account both compressive and extensional states of stress. This criterion is more conservative than the simpler criteria often considered (see Figure 4).

- The total stress was taken into account according to the Terzaghi principle, i.e. with a Biot coefficient equal to 1, which also maximises the risk of dilation occurring.

When considering the total stress for the dilation criterion, the cavern-scale simulations for the planned end situation of the caverns (end of mining in 2040) show that a dilatant zone of several metres can be observed at certain times around the cavern walls, more in the lower section of the caverns. There is no dilation in the core of the pillars, or in the salt roof which is a very thick (> 200 m) intact salt bed.

An example from LOCAS (simulated with planned end shapes of caverns) is shown in Figure 5 and Figure 6. This example shows that the Factor of Safety (FOS) for the onset of dilation is always greater than 1 in the core of the pillars and in the salt roof between the caverns and the overburden. The caverns can therefore be considered to be mechanically stable, with no risk of collapse due to dilation.

We also evaluate the Factor of Safety (FOS) in the dome-scale simulations at systematically placed query points adjacent to the cavern walls (Figure 7). This approach allows us to analyse the temporal evolution of the FOS during distinct phases of the cavern life cycle. Figure 8, illustrates the FOS evolution across the entire solution mining cavern field, providing insights into the stability and risk dynamics over time. Here, we pick the lowest FOS at a time and for each depth level, respectively. It therefore shows the most conservative FOS that occurs with respect to time and depth.

During the mining phase, where halmostatic pressure conditions are prescribed for the caverns, the Factor of Safety (FOS) remains above 1. During the waiting period, the FOS increases slightly, reaching a marginally higher level. At shut-in, when the cavern pressure is reduced to halmostatic conditions for cementing, the FOS drops close to or below 1, indicating that dilation is likely to occur at this stage. As the cavern pressure increases again, the FOS rises significantly, reaching values greater than 2 at the cavern roofs and even higher levels (>> 50) at mid-depths of the caverns. Even in the case of hydraulic fracturing (see Section 3.6), the overall stability of the cavern system is not compromised (i.e. a small fracture cross section can already transport enough brine to rapidly lower the pressure but will have no noticeable effect on the stability of the pillars or salt roof).

Figure 9 shows the same analysis as Figure 8, but for all caverns. It demonstrates that the characteristic patterns during the mining, waiting, and abandonment phases are similar across the different caverns.

Figure 10 presents the FOS mapped on to a horizontal cross section at the year 2250, providing a spatial perspective of the stability conditions across the field. The results highlight areas with enhanced FOS values, which are strongly correlated with mechanically distinct units within the salt dome and along its flanks. These correlations underscore the influence of local geological features.

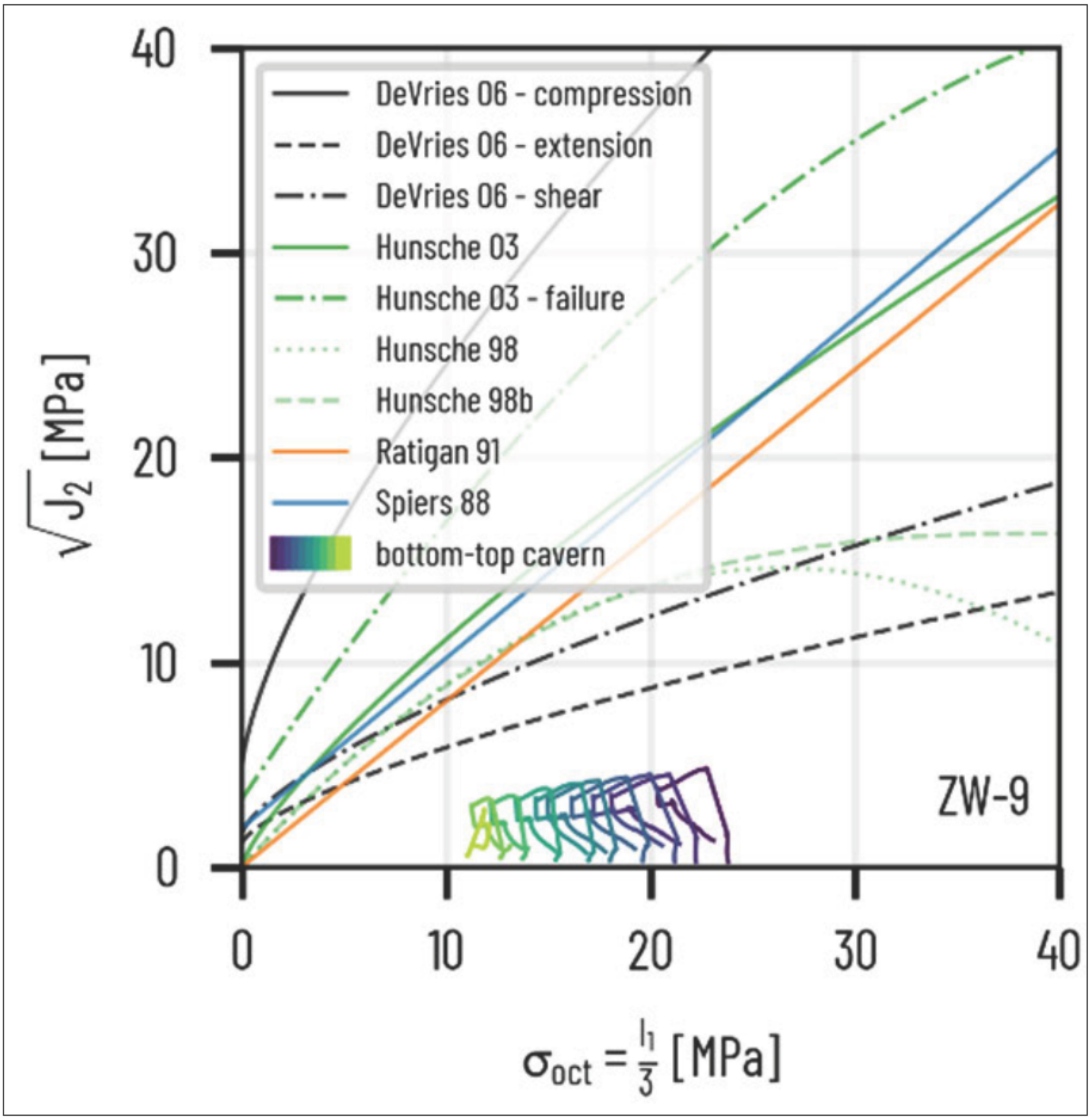

Figure 4. Evolution of the state of stress in the plane of invariants, mean stress on the horizontal axis and shear stress on the vertical axis, of the sT 3D dome-scale model (simulation B5). Assessment of dilation criterion at a 25 m offset from the ZW-9 cavern wall over the entire cavern lifecycle and across all depth levels within the ZW-9 depth range (color-coded). Even the most conservative dilation criterion is never met.

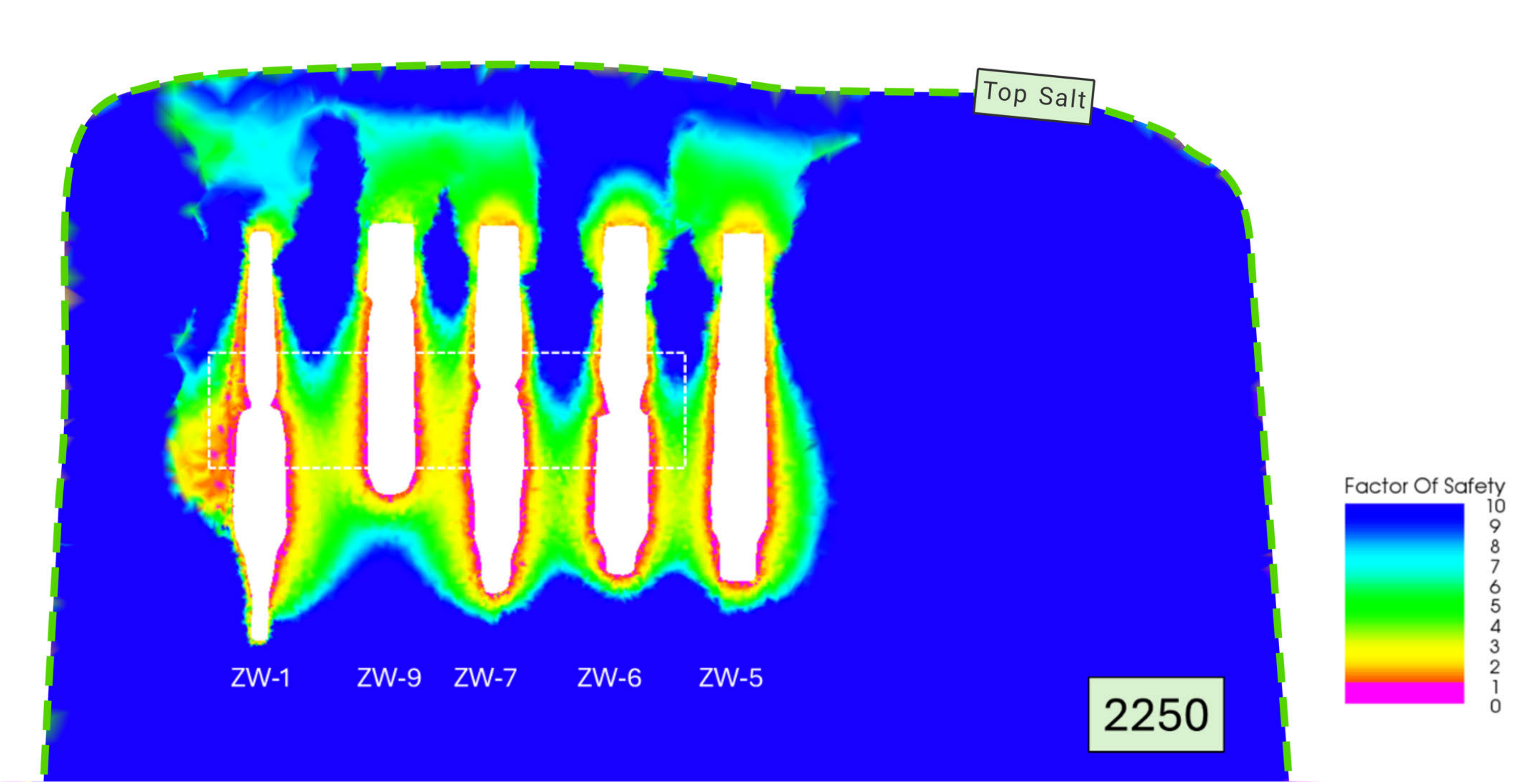

Figure 5. LOCAS 3D Model - Nobian caverns - Vertical section, in a plane passing through the axes of the ZW-1 and ZW-5 caverns, of dilation FOS contours in year 2250. The effective stress tensor is considered to evaluate the possible onset of dilation and a Biot coefficient of 1 is taken into account. As the FOS is only applicable for the rock salt, FOS is not displayed in the overburden.

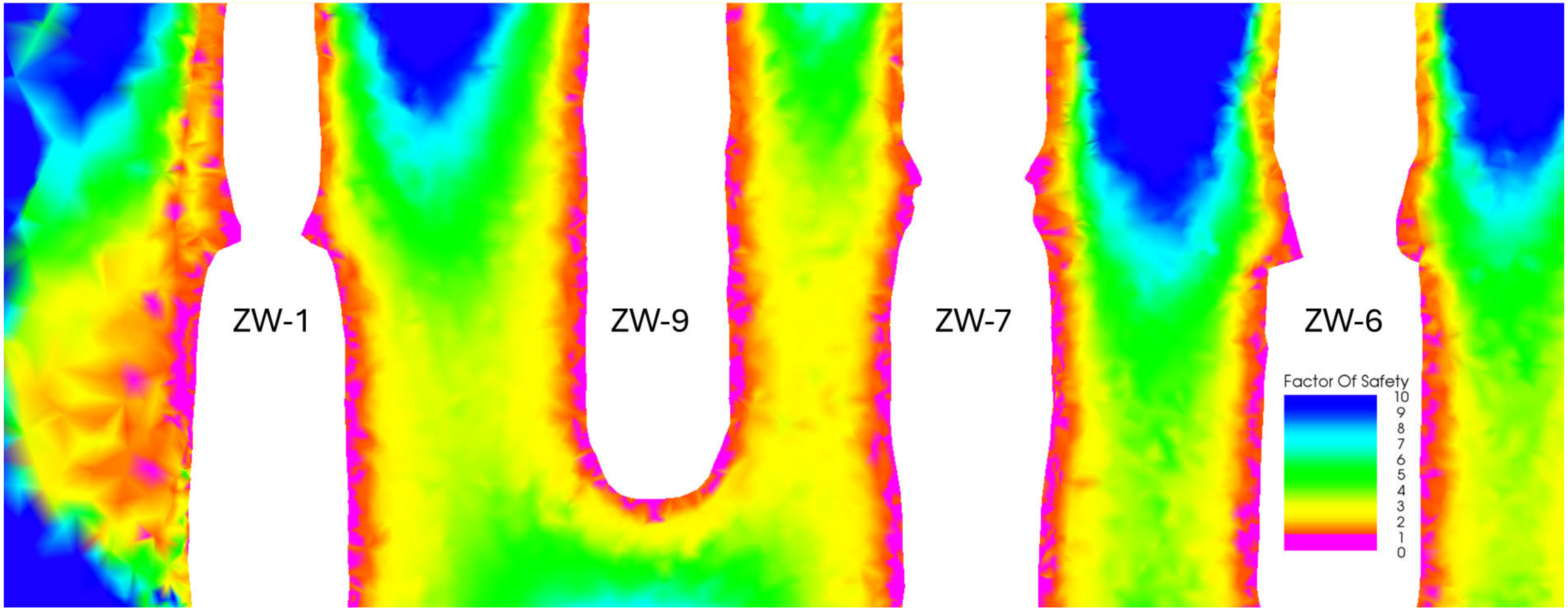

Figure 6. LOCAS 3D Model - Nobian caverns - Vertical section, in a plane passing through the axes of the ZW-1 and ZW-5 caverns, of dilation FOS contours in year 2250. The effective stress tensor is considered to evaluate the possible onset of dilation and a Biot coefficient of 1 is taken into account [Zoom].

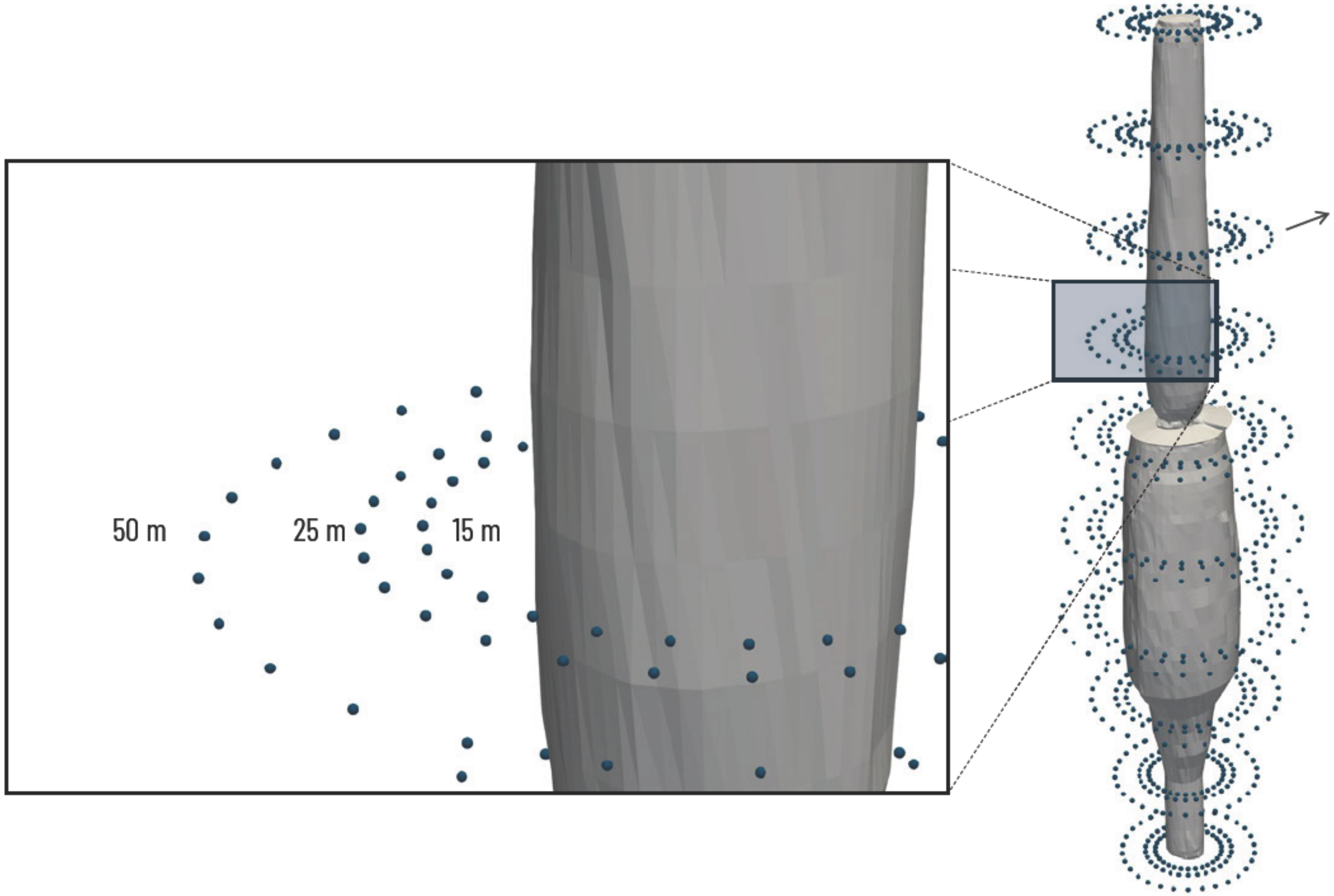

Figure 7. Systematic placement of query points adjacent to the caverns. Query points are arranged across 10 depth levels at defined offset distances of 15 m, 25 m, and 50 m from the cavern walls, respectively, to facilitate detailed analysis. For example, to display FOS over time, we extract the minimum FOS for each depth level and timestep, respectively, and plot it over time. For Δp, we take the maximum value per depth level and display it over time. This ensures that in the most conservative case is processed in the following evaluation.

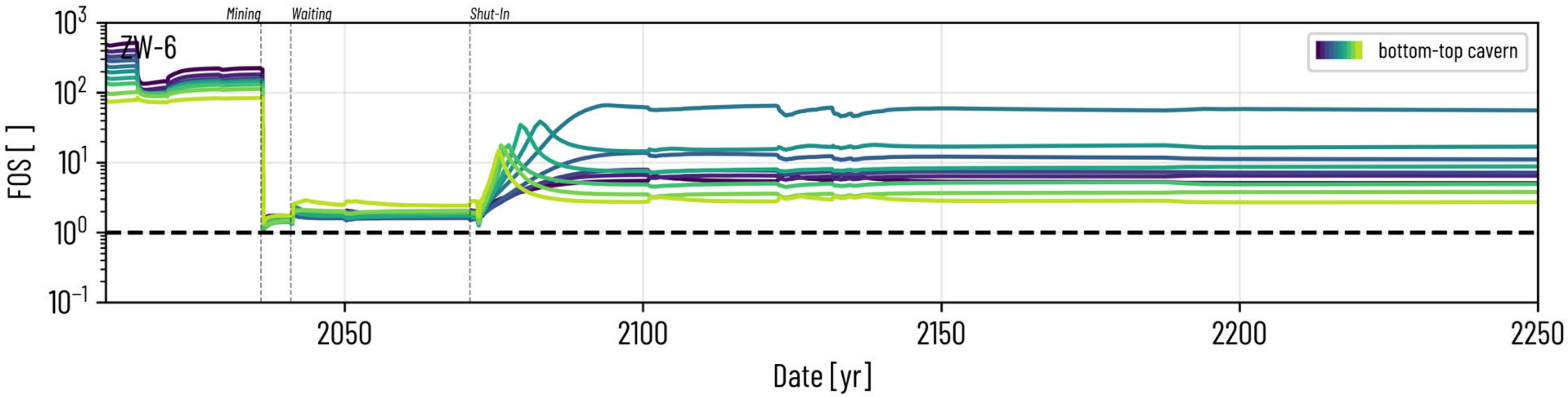

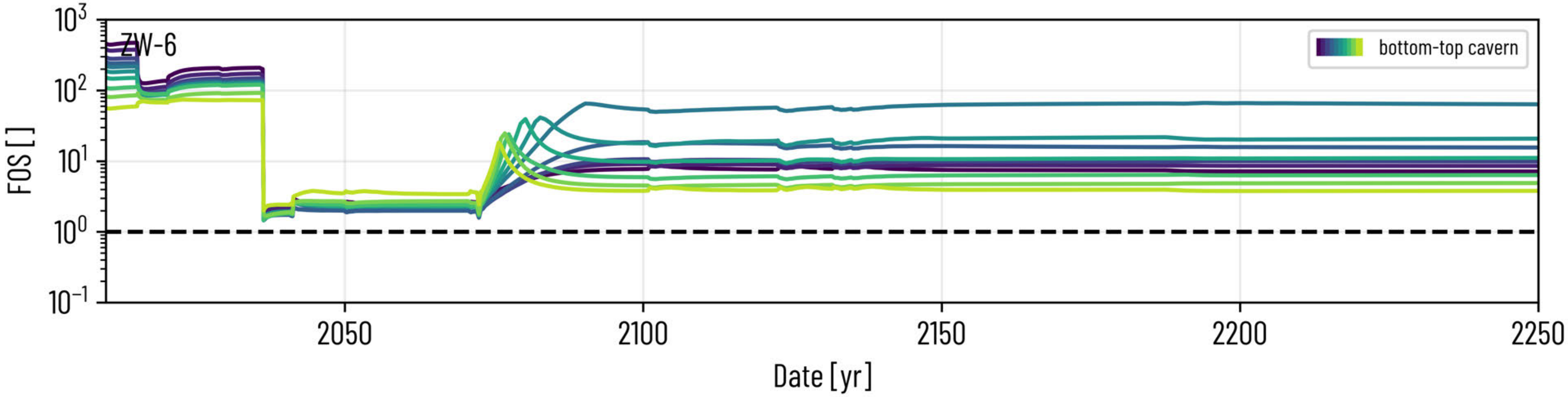

Figure 8. Assessment of FOS criterion at the cavern wall of ZW-6 over the entire cavern lifecycle and across all depth levels within the ZW-6 depth range (color-coded). TOP shows situation at cavern wall, BOTTOM represents the state at 25 m offset from cavern wall. During mining and waiting the Factor of Safety is lowest. It increases with the increase in cavern pressure during abandonment. In the equilibrium stage the FOS is smallest in the roof area and largest at mid cavern depth (sT 3D Dome-Scale Model, simulation I).

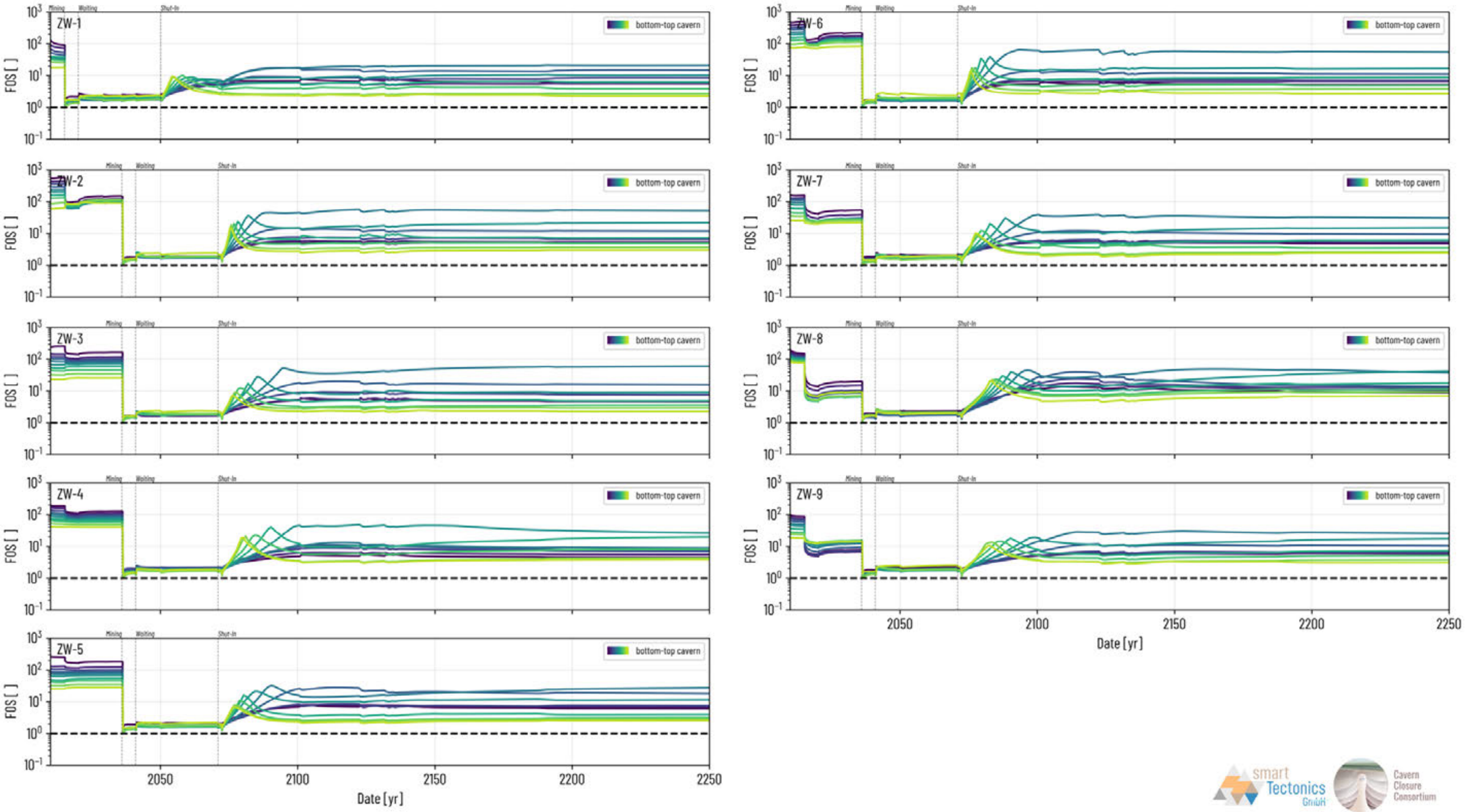

Figure 9. FOS evolution of all ZW solution mining caverns for simulation I, as shown for ZW-6 in Figure 8 (bottom). The evolution of the FOS for dilation is shown throughout the full cavern lifecycle at the cavern wall (0 m offset) across specific depth levels (as indicated in Figure 7). While conditions for dilation onset are occasionally met during the waiting period up to the start of abandonment, the FOS magnitude consistently increases over time during the abandonment phase. Safest conditions are reached ad mid cavern depths. Lowest FOS are reached in the upper cavern parts during the equilibrium phase of the caverns. High resolution figures are provided as appendix.

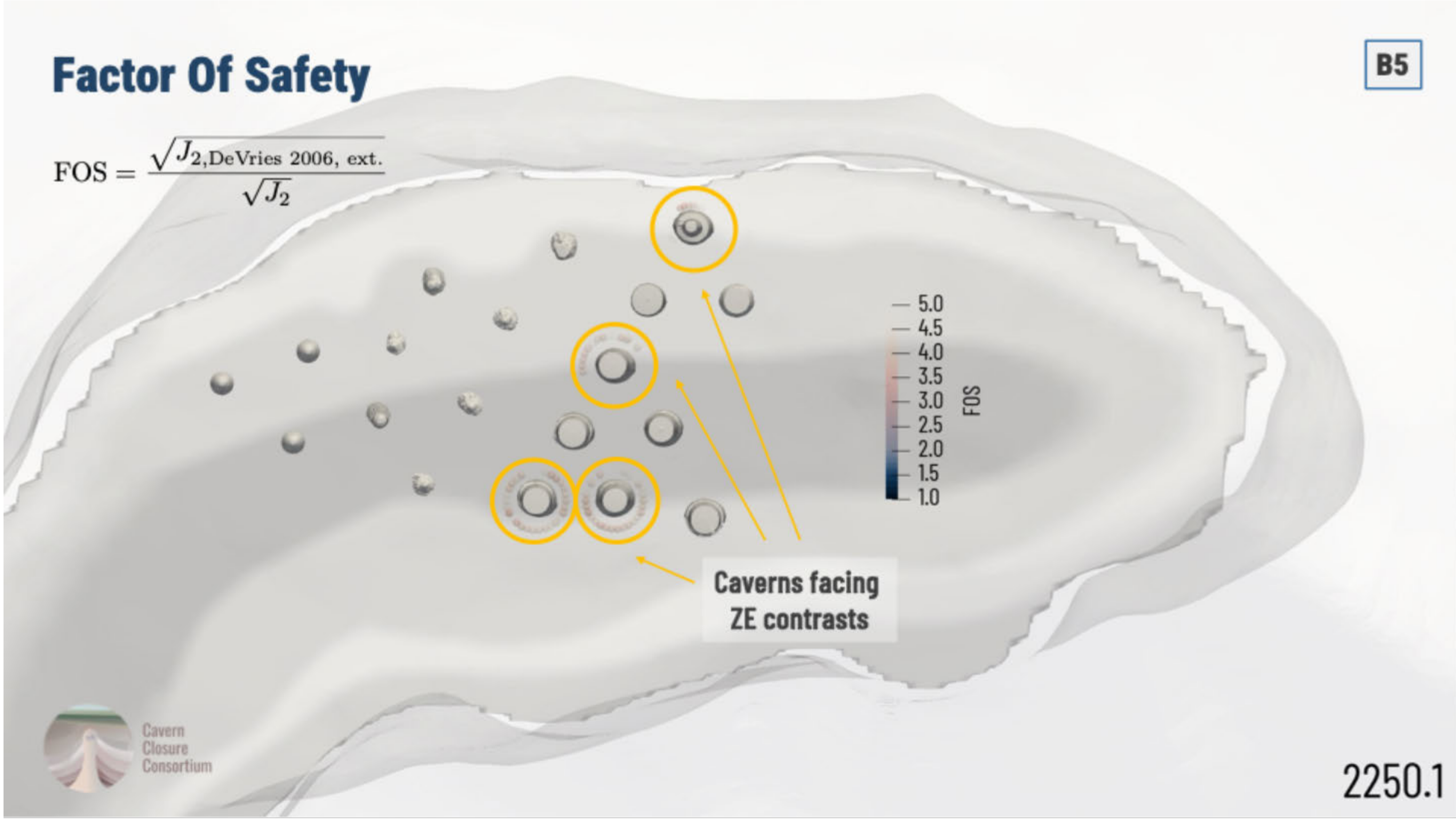

Figure 10. LaMEM 3D dome-scale model, simulation B5. Horizontal section in the long-term abandonment phase of the cavern, 2250 (end of simulation time). FOS is assessed at query points in 50 m offset from cavern walls across several depth levels ranging from cavern bottom to cavern roof (see Figure 7). FOS is smaller for caverns that face mechanically distinct Zechstein units (illustrated in grey scales) or, adjacent salt dome flank.

2.5 Conclusions regarding of Zuidwending caverns

The probability of the formation of a sinkhole in Zuidwending is negligible (i.e. estimated to be smaller than 10^{-6}[†]) and can realistically be ruled out. Unlike Bayou Corne and Sulphur Mines, all caverns have a regular shape and are, in the realistic interpretations, more than a hundred metres from the sides of the dome. Furthermore, the caverns are relatively deep with a very thick salt roof, significantly distancing them from the overburden. Therefore, given the configuration of the Zuidwending cavern field, no realistic process is imaginable that could lead to the formation of a sinkhole during the entire lifecycle of the cavern field, including the abandonment phase.

Collapse is not a possibility due to dilation, as this does not propagate into the core of the pillars or the thick salt roof. Even if hydraulic fractures would appear in the walls or roofs of the caverns, this provides sufficient structural stability.

3 Assessment of the Likelihood of the Onset of Hydraulic Fracture

3.1 Summary

This section evaluates the potential for hydraulic fracturing throughout the cavern life cycle, considering key stages such as mining, waiting, and abandonment. The assessment is based on numerical simulations, expert knowledge, and field data, particularly from the Etzel test.

Prior to abandonment, pressure decreases to halmostatic conditions for cementing can result in very localized dilation and permeation in the vicinity of the cavern wall. However, the likelihood of hydraulic fractures propagating beyond 15 meters remains negligible (estimated to be lower than 10^{-6}). After abandonment, permeation becomes more prevalent, especially near the cavern wall and roof. In the first months to years, when pressure increases at a relatively high rate, small-scale hydraulic fracturing is not excluded, though its propagation remains highly localized at the cavern wall. The probability of a large subvertical fracture propagating beyond 15 meters from the cavern wall can be estimated as improbable (estimated order of magnitude between 10^{-4} and 10^{-5}). Over the long term, as cavern pressure increases and brine warming decreases, permeation may persist, but the likelihood of significant hydraulic fracture formation diminishes further. While hydraulic fractures cannot be entirely ruled out, the probability of a large subvertical fracture propagating beyond 15 meters from the cavern wall becomes very unlikely (estimated order of magnitude between 10^{-5} and 10^{-6}).

After considering several scenarios and the planned end volume of a representative cavern, it appears that the volume of brine that could escape from the cavern to surrounding layers through one of several fractures remains very limited, ranging from 540 m^3 to 8,600 m^3.

3.2 Introduction

This section explores the onset of hydraulic fracturing in the context of salt cavern abandonment, particularly focusing on the limitations of traditional geostatic stress concept

[†] According to Nobian document 12.01.6.OP11 Hazard Studies (page 18, figure 8). These type of risks may be estimated qualitatively based on the combination of frequency/likelihood and severity.

as an evaluation reference for cavern pressure and the need to adopt least principal compressive stress (σ_3) as a standard for evaluation.

In the context of cavern stability and hydraulic fracturing risk assessment, likelihood refers to the probability or tendency of an event occurring under given conditions. In our assessment, it is a qualitative measure derived from numerical simulation results, expert knowledge, and literature. Through this combined approach, we aim to evaluate the likelihood of fluid permeation or hydraulic fracturing within the salt cavern system, considering stress and pore pressure conditions, as well as structural deformations that may lead to mechanical dilation.

The section is structured as follows:

- Definitions of key physical parameters to establish a common understanding.
- Difference between permeation and hydraulic fracturing
- A discussion on why the concept of geostatic stress fails in salt domes and the necessity of adopting a new standard.
- Consequences of opening a hydraulic fracture
- A summary table consolidating observations, simulation findings, and evaluations for further risk analysis

3.3 Physical Parameters involved in Hydraulic Fracture Risk Assessment

To ensure clarity and consistency, we re-iterate the meaning of the physical parameters involved in the evaluation of hydraulic fracturing risk.

Geostatic Stress, $\boldsymbol{\sigma_{geo}}$

The stress exerted by the weight of overlying rock strata. It is often used as a reference in stress analyses outside of salt domes, where sub horizontal lithology prevails and one of the principal stresses can be approximated as subvertical (commonly referred to as σ_{geo}).

However, it is essential to recognize that geostatic stress is a theoretical concept that does not hold true within the context of salt domes and does not serve as a reliable approximation for least compressive principal stress. In the following section, we outline the reasons why relying on geostatic stress to evaluate hydraulic fracturing risks in salt domes can lead to inaccurate and potentially misleading assumptions.

Note that we use σ_{geo} as a normalization constant in our evaluation analysis to facilitate comparisons with established reference quantities.

Least Principal Compressive Stress, $\boldsymbol{\sigma_3}$

In our study, we use the convention that stresses are negative in compression, which is the common sign convention in geomechanics (i.e., Jaeger, Cook & Zimmermann, 2007). In the context of the stress-driven infiltration of brine into the salt host rock (permeation) and hydraulic fracturing, the pore fluid pressure of the brine must exceed σ_3 in order to initiate the opening of grain boundaries in the salt rock (Schmatz et al., 2024).

Tensile Strength, $\boldsymbol{T_0}$

Additionally, the fluid pressure (P_f) must also overcome the salt's tensile strength T_0, typically around 1.5 MPa, for hydraulic fracturing to occur (DeVries et al., 2022).

Leak-off Conditions

In classical leak-off tests in wellbores (LOTs, Figure 12, e.g. White et al., 2002), the Leak-Off Pressure (LOP) represents the fluid pressure required to exceed the least principal compressive stress σ_3 and initiate micro-fractures and permeation into the host rock, marking the onset of tensile stress effects. For a fracture to propagate, however, the fluid pressure must also surpass the tensile strength of the rock (T_0). In the context of a LOT, the pressure required to propagate a fracture is referred to as Formation Breakdown Pressure (FBP).

To summarize the fluid pressure and associated least principal compressive stress in a single term, we define Δp:

$$\Delta p = P_f - \sigma_3$$

The onset of permeation and hydraulic fracturing can be expected under the following conditions:

$\boldsymbol{\Delta p < 0, \Delta p \to 0}$**:** Laboratory experiments (Popp et al., 2007, 2012) indicate that permeation occurs as a smoother process, influenced by the salt's local tensile strength and inherent heterogeneities. It is generally accepted that the probability of transition to permeation increases as Δp approaches zero.

$\boldsymbol{\Delta p = 0}$**:** Represents the threshold at which fluid pressure is sufficient to initiate permeation and grain boundary opening.

$\boldsymbol{\Delta p > T_0}$**:** At this condition, hydraulic fracturing is likely to occur as the fluid pressure exceeds both σ_3 and the tensile strength T_0.

There are several ways to describe the pressure driven permeation onset, as outlined above. Figure 11 illustrates how permeation is modelled in both dome-scale and cavern-scale simulations. While in cavern scale simulations, the IUB criterion is used (Rokahr et al., 2002), whereas dome-scale simulations use a smooth transition based on a tanh-function. I both cases, the modelling parameters are adjusted to align to ensure the best possible alignment between the two approaches.

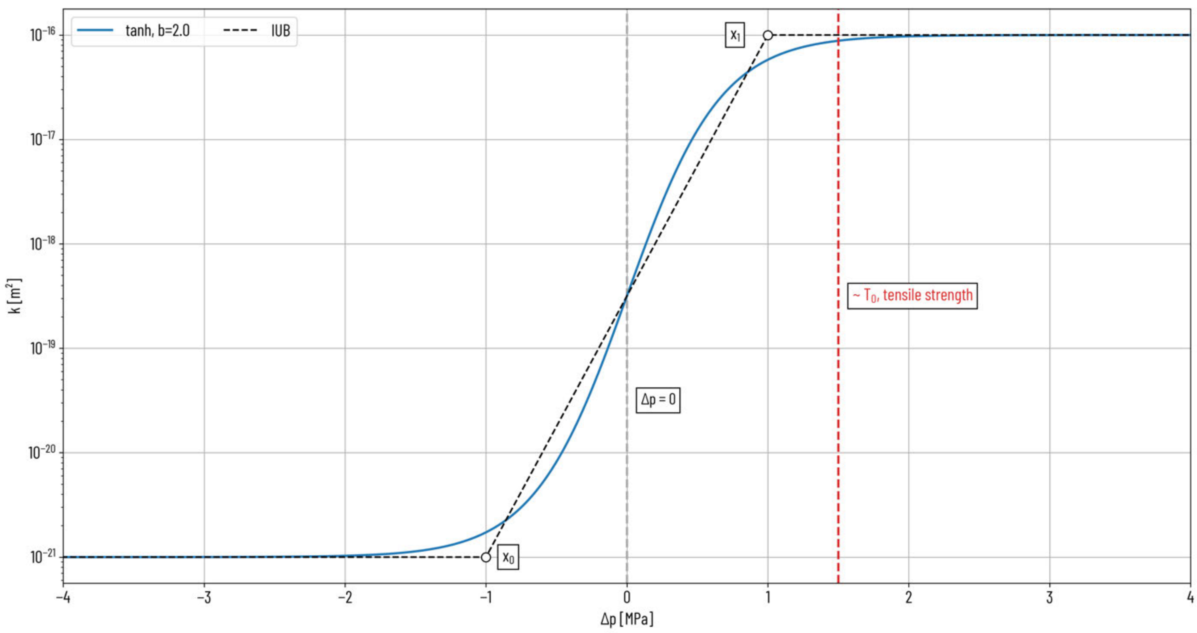

Figure 11. Permeation criteria implementations. In cavern scale simulations, the IUB criterion is applied, while in and dome-scale simulations a smooth tanh function is used to model the pressure-driven permeation onset.

Geostatic Stress vs. Principal Stresses in Different Geological Settings

In **flat-bedded sedimentary environments** (e.g., the Netherlands), vertical stress (σ_V) is typically assumed to be one of the principal stresses due to horizontal stratigraphy. In most regions of the North Sea, a normal faulting stress regime exists, meaning:

$$\sigma_V > \sigma_H > \sigma_h,$$

where (i.e. $\sigma_V = \sigma_1 \geq \sigma_H = \sigma_2 \geq \sigma_h = \sigma_3$).

Although local stress perturbations can occur, one of the principal stresses is generally assumed to be vertical (σ_V), and it can be computed by integrating the bulk density over depth (z):

$$\sigma_V = \int_0^z \rho(z) g \, , dz$$

In the context of cavern engineering the vertical stress is often referred to as "**Geostatic Stress**", i.e. $\sigma_V = \sigma_{geo}$.

In **flat-bedded salt formations,** the assumption of an isotropic stress state often applies:

$$\sigma_V = \sigma_H = \sigma_h = \sigma_1 = \sigma_2 = \sigma_3$$

This allows for a direct relationship between cavern equilibrium pressure and geostatic stress:

$$\sigma_V = \sigma_3 = \sigma_{geo}$$

However, **in the case of a salt dome**, the concept of $\sigma_V, \sigma_H, \sigma_h$ is no longer valid, as none of the principal stresses remain vertical due to the complex deformation history and the geometry of the salt dome where the salt sediment interface acts as a tangential-stress free boundary.

While the hypothetical σ_{geo} (geostatic stress) can still be computed as the integral over bulk density, it is no longer a principal stress within the salt dome. Instead, numerical modeling results show that the true σ_3 can be higher than σ_{geo} inside a virgin salt dome, even without caverns (Baumann et al. 2019, KEM-17, dome-scale report). In absolute terms, these differences are typically small (1-3 MPa) but become more pronounced with cavern emplacement.

Time-Dependent Evolution of σ_3 in a Salt Dome in proximity of Caverns (Confinement)

When caverns are introduced, an additional time-dependent component is introduced to σ_3. Unlike in a virgin salt dome, where σ_3 is relatively stable, cavern operations significantly alter the stress evolution over time.

Most importantly, σ_3 becomes a function of the time-dependent cavern pressure $P_c(t)$:

$$\sigma_3 = \sigma_3(t) = \sigma_3(P_c(t))$$

As the cavern pressure evolves over time, the difference between σ_3 and σ_{geo} increases, often exceeding the 1-3 MPa range observed in virgin salt domes. This effect is particularly relevant during cavern abandonment, where elevated equilibrium pressures increase σ_3 significantly in proximity of the caverns. We refer to this effect as the **confinement of the host rock**, a critical factor that must be accounted for in the risk assessment of hydraulic fracturing in salt caverns.

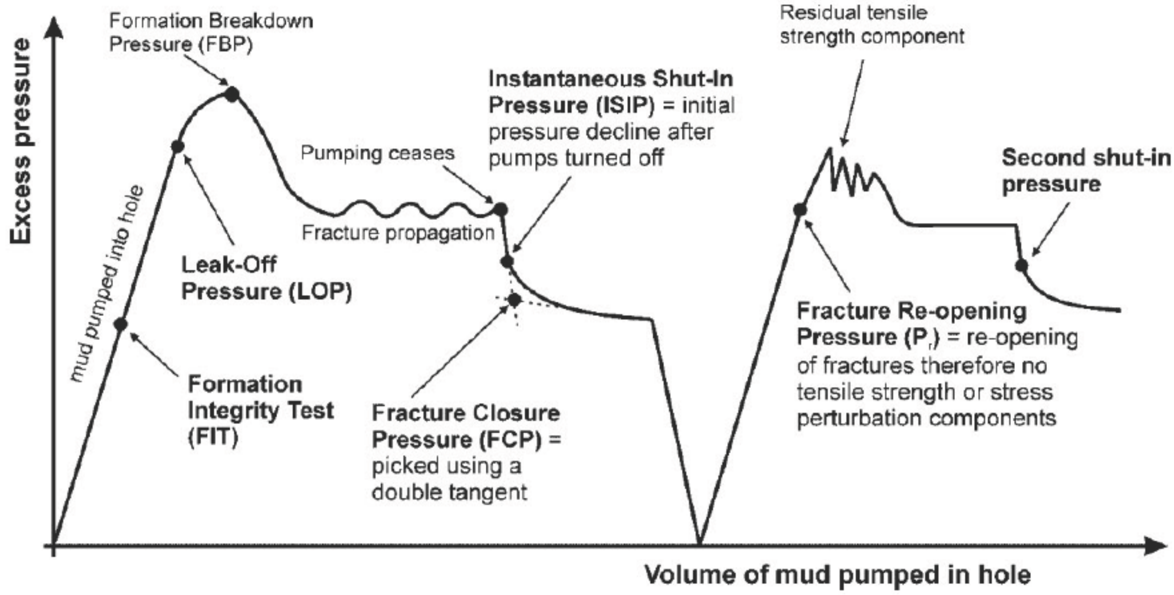

Figure 12. Classical viewpoint of Leak-Off Test with Leak-Off-Pressure and Formation Breakdown Pressure, where it is assumed that LOP is an approximation of the pressure required to initiate microfractures or permeation into the host rock, and FBP is the pressure that is required to be exceed also the tensile strength of the rock and initiate fractures, thus $LOP + T_0 \approx FBP$. White et al. (2002).

It is essential to differentiate between permeation, which involves the slow, pressure-driven opening of grain boundary pathways, and hydraulic fracturing. While both processes occur under comparable stress and pressure conditions, the key distinction lies in the rate of pressure increase. A rapid pressure rise is likely to result in hydraulic fracturing, whereas a slower, more gradual pressure increase facilitates permeation. This gradual process allows for the viscoelastic relaxation of the rock salt and the eventual healing of the salt host rock, as supported by microstructural evidence (Debois et al., 2012; Houben et al., 2013).

Dilation and its relationship with permeation and hydraulic fracturing

In our understanding, hydraulic fracturing is a progressive process that begins with dilation, where micro-fractures form and locally increase connected porosity. Note that dilation occurs not only in mining situations but also as a naturally occurring process. This process, along with the presence of some locally connected porosity, contributes to a certain degree of permeability in rock salt, albeit very low (e.g. Schoenherr et al., 2007; Zijp et al., 2018). Dilation reduces the residual tensile strength of rock salt, facilitating the initiation of brine permeation. As pressure increases—governed by both its magnitude and rate of increase—some dilatant micro-fractures become more localized, potentially leading to the formation of a hydraulic fracture (see KEM-17, Urai & al., 2019, Figure 62 page 69).

Therefore, in evaluating the numerical modeling results, special attention is also given to the occurrence of dilation. This is assessed using the Factor of Safety (FOS), based on a conservative criterion (e.g., DeVries, 2006). For more details, refer to Section 2.

3.4 Permeation and hydraulic fracturing

This section is thought as a more general discussion

3.4.1 The KEM 17 perspective

As mentioned in the KEM-17 report: *The formation of micro-fractures when cavern pressure is close enough to geostatic pressure can be considered a certainty. This is proved by the increase in the cavern compressibility during the Etzel test (see section 3.4.2), which remains approximately constant until a threshold pressure ("leak-off pressure") is reached.*

As shown by Berest et al. (2016) for the cooling of a gas-filled cavern, we can expect the initial development of numerous small fractures (micro-fracking) whose length will increase with the pressure in the cavern. But after a while, if the increase in pressure continues, only certain localised fractures will continue to develop, while the others will close.

This micro-fracking process is much smoother than what can be observed during a standard fracture test. In a borehole, during a standard fracture test, when the fracture breakdown pressure is reached (onset of a fracture), borehole pressure drops (Figure 12). This is because a borehole is a very stiff cavity, and the volume of the brine that enters the fracture is not negligible when compared to the volume of the borehole. The same is not true for the occurrence of a hydraulic fracture in a full-size cavern whose volume is larger than a borehole volume by three to five orders of magnitude. This is a difficult point in any test of this kind. It is highly likely that, when cavern pressure increases, the number and length of these micro-fractures increase. It is not impossible that, after some time, localization takes place: most micro-fractures stop growing, a small number of the micro-fractures keep growing (their aperture and their length increase), leading to the formation of "hydraulic fractures".

3.4.2 The Etzel Test

The Etzel K-102 test, conducted in Germany from 1990 to 1993, was a landmark in-situ experiment designed to investigate the behaviour of salt caverns under pressure during abandonment (Denzau et al., 1994; Staudtmeister & Rokahr, 1994). The test was performed on a brine-filled cavern located at a depth of 850 m, the deepest point is circa 1500 m, with a volume of 233,000 m^3.

The main objective was to gradually increase the cavern pressure up to a gradient of 0.32 bar/m, which was believed at the time to be a safe maximum pressure for abandoned caverns if reached slowly enough. However, the test revealed unexpected behavior: although the pressure increase rate was relatively slow (maximum 0.36 bar/day), the cavern began showing signs of permeability increase at pressure gradients much lower than anticipated. Specifically, the apparent cavern compressibility started increasing significantly during the second pressure step (0,190 - 0.205 bar/m), well below the estimated geostatic gradient of 0.211-0.240 bar/m. The test had to be stopped when, during the fourth pressure step, cavern pressure began dropping despite continued brine injection (Figure 13). While continuously injecting brine, pressure could not be increased above a gradient of 0,226 bar/m and decreased to 0,221 bar/m.

During the test, a notable increase in cavern compressibility was observed as pressure built up (Djizanne et al., 2012). The initial compressibility coefficient was relatively low at 3.7×10^{-5} /bar during the first pressure step, reflecting the normal elastic behavior of the cavern system. However, this coefficient increased significantly to 4.7×10^{-5} /bar during the second pressure step and further increased to 5.7×10^{-5} /bar during the third step. This progressive increase in apparent compressibility indicates that the cavern was no longer behaving as a purely elastic system, even if locally at the cavern wall the rock salt becomes softer because of microcracks. When pressure is low, cavern compressibility primarily reflects the elastic properties of both the brine and surrounding rock mass. The observed increase in apparent compressibility at higher pressures, while still below geostatic pressure, suggests the development of additional phenomena - likely the onset of increased permeability or micro-fracturing in the salt mass surrounding the cavern. This interpretation is supported by the fact that pressure eventually began decreasing during the fourth pressure step despite continued brine injection, indicating significant brine penetration (more than the 7 m³ per day constant pump rate) into the rock mass.

The key finding from this test was that salt permeability at the cavern wall can increase substantially even when cavern pressure remains below geostatic pressure. This challenged the prevailing theory of the time. The results supported laboratory observations suggesting that salt permeability increases when fluid pressure exceeds the minimum compressive stress at the cavern wall. Furthermore, the test demonstrated that the history of cavern pressure plays a crucial role - the long period of low pressure operation before the test may have led to stress redistribution that made the cavern more susceptible to permeability increases during subsequent pressurization.

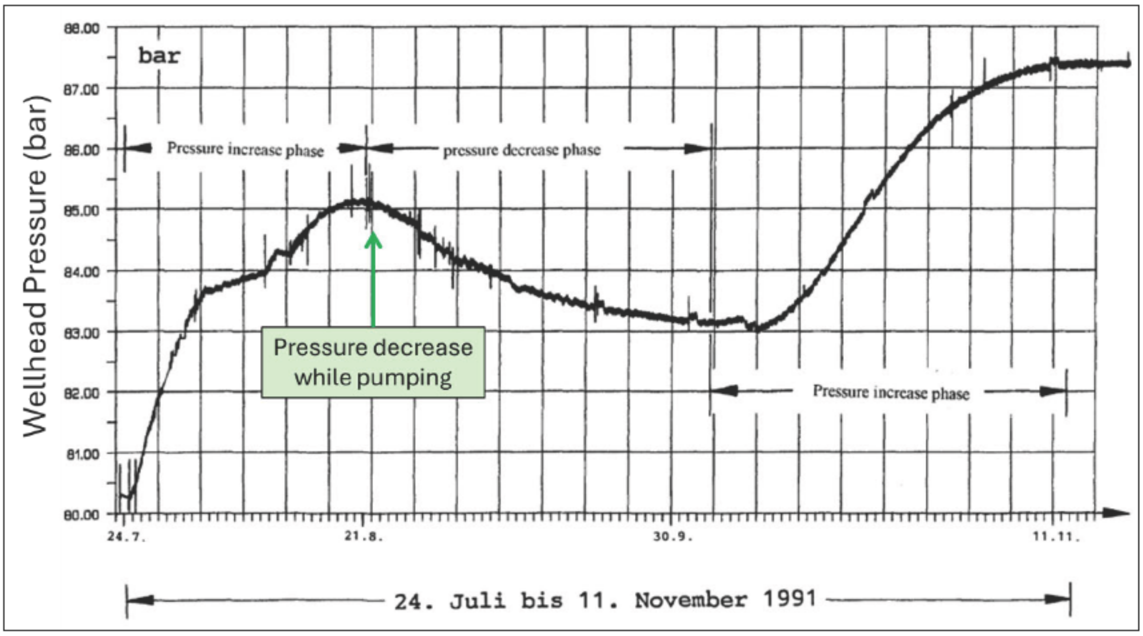

Figure 13. Wellhead pressure evolution during Etzel test (After Staudtmeister & Rokahr, 1994.)

From seismic monitoring data during the Etzel test, one can conclude that both permeation-driven processes and larger progressing fractures are likely to have occurred. The seismic data from the test phases reveal distinct patterns in event distribution, indicating different fracture mechanisms at play. During all the different pressure increase phases, the highest number of events occurred at the cavern roof and just below it, suggesting intense micro-fracturing and stress-induced permeation along the cavern walls, while activity near the casing shoe remained minimal. In contrast, pressure reduction phases saw a surge in seismic activity in the upper cavern region, likely associated with larger fractures and stress relaxation. Notably, low-frequency events, potentially linked to larger-scale fractures, were predominantly recorded during these phases (Ford & Dreger, 2020), indicating that significant structural adjustments occur as pressure decreases (Figure 14). During quiet phases, a high number of events persisted below the cavern roof, indicating that stress redistribution and micro-fracturing continued even in stable conditions. Small high-frequency events were also present, particularly near the casing shoe, suggesting ongoing permeation-driven deformation. Overall, the seismic observations indicate that pressure reduction facilitates larger-scale fracturing near the cavern roof, while pressure increase primarily drives micro-fracturing and permeation processes along the cavern walls.

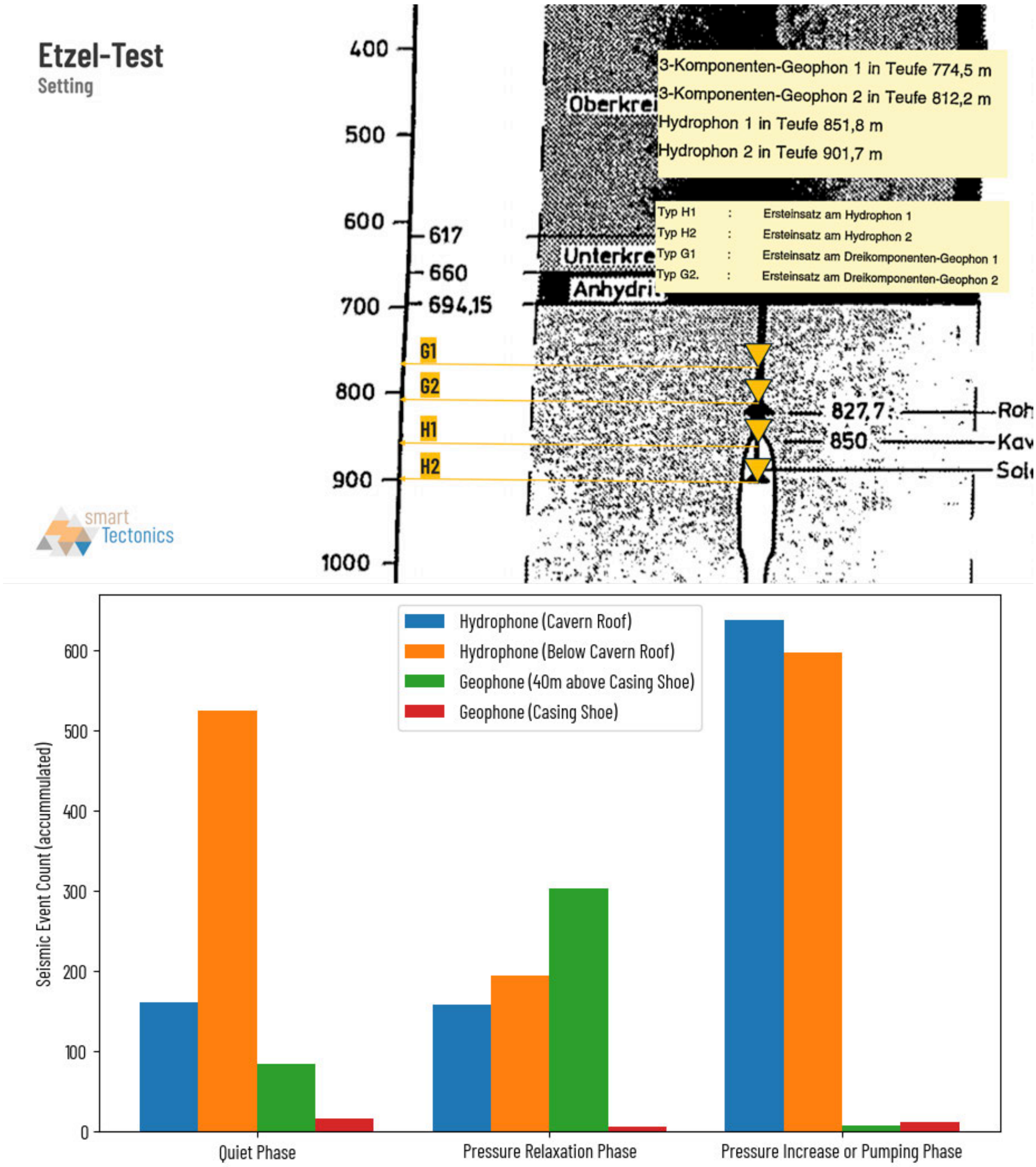

Figure 14 **Top:** Configuration of geophones and hydrophones used for seismic monitoring during the Etzel test (modified from Denzau et al, 1994). **Bottom:** Distribution of occurring acoustic and microseismic events during the Etzel test.

3.4.3 Geomechanical Differences Between Veendam and Zuidwending Caverns: Implications for Fracturing

The salt solution mining caverns in Veendam and Zuidwending exist under fundamentally different geological conditions. The Veendam caverns are located within a salt pillow containing significant amounts of carnallite and anhydrite, while the Zuidwending caverns are part of a salt dome consisting primarily of relatively clean halite (Abandonment of solution mining cavern field Zuidwending, The Netherlands – an integrated, multiscale investigation, version 240411). Additionally, the Veendam caverns mine magnesium salts, which exhibit a much faster creep rate compared to the rock salt in Zuidwending. Another key difference is their depth: at Veendam, the caverns lie just a few tens of meters below the salt-sediment interface, directly beneath the highly permeable Buntsandstein formation, which introduces different mechanical and hydraulic constraints.

In 2018, a hydraulic fracture occurred in the salt roof of one of Nedmag's caverns in Veendam, despite operating at sub-geostatic cavern pressure. The primary cause was that salt roof stress had fallen below cavern pressure; a condition that developed over time due to prolonged low cavern pressure followed by a cavern pressure increase to slow surface subsidence. This stress reduction in the salt roof was strongly influenced by stress arching in the overburden, where decreasing vertical stresses led to a corresponding decrease in salt roof stress, ultimately triggering a fracture (Fokker and Smit, 2024).

The different geological conditions, the different type of salt and the depth cause significant differences between the geomechanical behaviours of the caverns in Veendam and Zuidwending, with Veendam's conditions making it more susceptible to stress-induced fracturing.

3.5 Why the Concept of Geostatic Stress not applicable in the Context of Cavern Abandonment

In the context of salt domes, the state of stress is highly disturbed. This occurs both outside the salt dome, where the salt-sediment interface (Top Salt) acts as a quasi-shear stress-free surface, perturbing the orientation and magnitudes of the principal stresses in the adjacent sedimentary rocks, and within the salt dome itself.

It is often incorrectly assumed that the stress state within salt domes is isotropic, with zero shear stress, leading to the false conclusion that geostatic stress is equivalent to the least principal compressive stress (σ_3). However, the geometry of the salt dome and the internal structural heterogeneities of the salt rock result in a non-uniform and non-isotropic stress state (Baumann et al., 2019; KEM-17 dome-scale report).

The emplacement of salt caverns introduces additional heterogeneities in the salt dome. Like the salt-sediment interface, the cavern walls act as tangential stress-free boundaries. Additionally, the normal stress acting on cavern walls is a time-dependent boundary condition that scales with cavern pressure during the cavern's operational lifetime.

Below, we demonstrate that a high equilibrium cavern pressure acts as confinement for the salt host rock, significantly increasing σ_3 during abandonment. This critical fact is often overlooked when cavern equilibrium pressures are compared against geostatic stress.

Figure 15 demonstrates the difference between σ_3 and σ_{geo} during abandonment at the end of the cavern-life time simulation (year 2250). The cross-section in the upper figure visualizes the ratio σ_3 / σ_{geo}.

σ_{geo} remains invariant to dynamic stresses in the dome, as well as to cavern operational and abandonment pressures over time. In contrast, σ_3 shows significant variations, being 10-20% larger in the vicinity of the caverns and exceeding by over 30% in close proximity (< 15 m) to the cavern walls. In absolute terms, σ_3 surpasses σ_{geo} by about 1 MPa on average, while near the cavern walls, this difference increases to around 3 MPa (Figure 15, bottom).

In the following section, we focus on the fracture risk associated with the cavern life cycle by examining its characteristic stages: mining, waiting, and abandonment. Particular attention is given to Δp (the pressure differential), the relevant σ_3 and how σ_3 evolves during these stages in relation to the pore pressure (see Geostatic Stress vs. Principal Stresses in Different Geological Settings above)

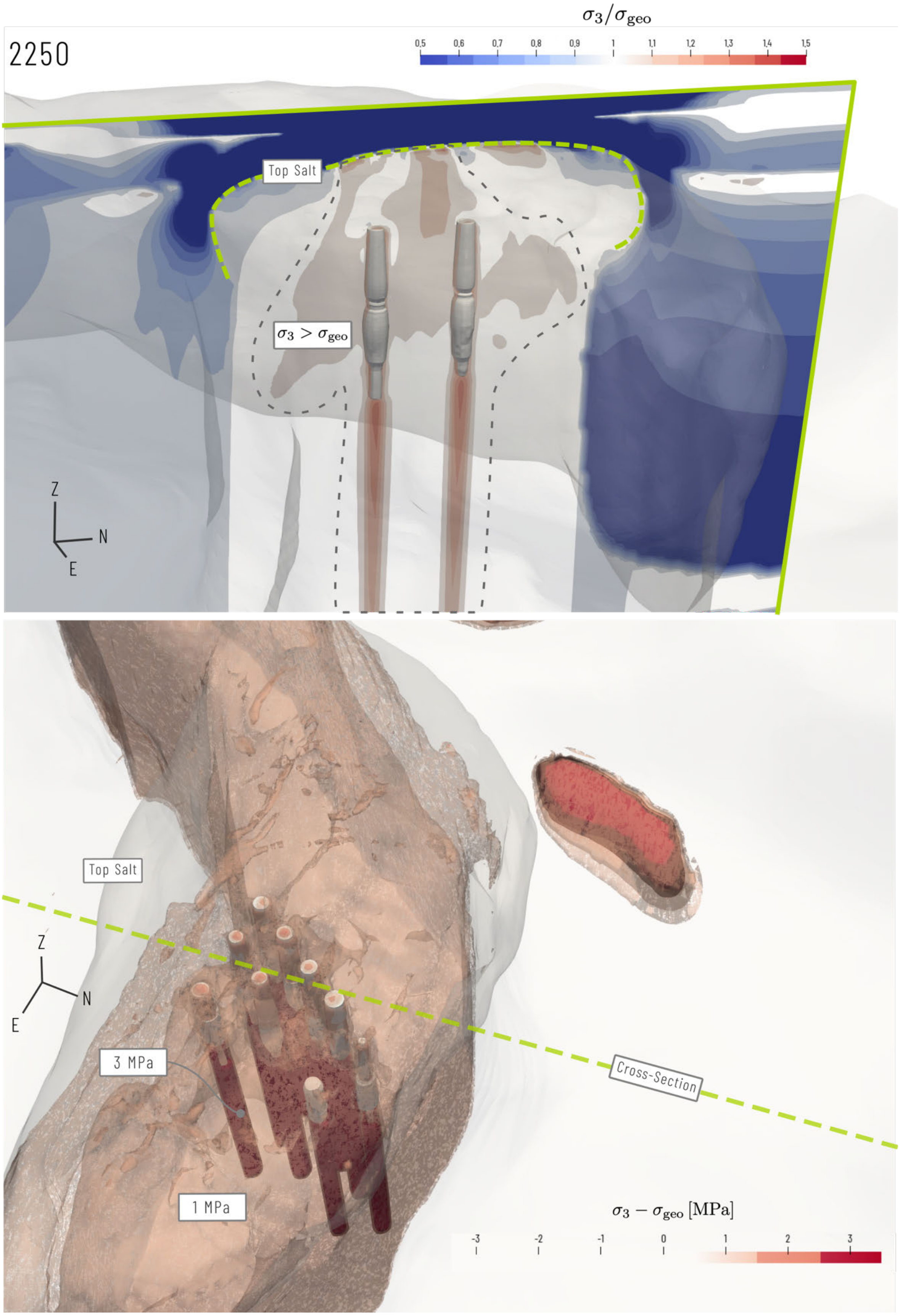

Figure 15. **TOP**: σ_3/σ_{geo} ratio at long-term abandonment (2250). The concept of geostatic or vertical stress is not applicable in the context of salt domes. While $\sigma_3 < \sigma_{geo}$ outside the dome, σ_3 is 10%-20% higher as σ_{geo}. **BOTTOM**: 3D perspective (from Northeast in SE direction) showing the absolute difference between σ_3 and σ_{geo} as contours inside the dome. For visibility, contours at negative differences are clipped as they are only present in the very top corners of the dome and outside the salt dome.

3.6 Hydraulic Fracture Potential at Different Stages of the Cavern Life-Cycle

In this section, we examine the fracture potential throughout the cavern life-cycle, focusing on the key stages: mining, waiting, and abandonment. Each stage presents unique stress conditions and fracture risks, influenced by the interplay between the least compressive principal stress (σ_3) and the fluid pressure (P_f).

Generally, 2D and 3D cavern-scale calculations indicate that, in some areas, cavern pressure at the wall can exceed the least compressive principal stress and the salt's tensile strength. This may cause microfractures, locally increasing permeability—and possibly porosity—resulting in a minor brine leak that reduces pressure buildup. Simulations predict an overall pressure increase of less than 0.05 bar/day.

The creep behaviour of the salt is well-constrained through a probabilistic approach, ensuring robust stress predictions. Additionally, within the CCC approach, cavern life cycles are also modelled at the dome-scale to provide the most accurate estimates of stress states and boundary conditions. This allows for a precise assessment of stress evolution around the cavern field, extending toward the salt-sediment interface and beyond. As a result, we have high confidence in the reliability of σ_3 predictions at the cavern field location, which has strong implications for the onset of permeation and hydraulic fracturing.

A key factor in the assessment is the least compressive stress (σ_3). Figure 16 illustrates how σ_3 evolves throughout the cavern life cycle at a 15 m offset from the cavern wall, using ZW-7 as an example, with a focus on the roof and bottom sections. Figure 17 provides context by comparing this evolution to the associated P_f. Characteristic values of σ_3 and corresponding P_f were extracted from the distinct life-cycle stages in Figure 16 (i.e., mining, waiting, abandonment) and analysed across all caverns in the field, considering depth variations and offset distances from the cavern wall. The results are presented as scaled quantities to emphasize the relationships and relationships between σ_3, P_f, and the characteristic cavern life-cycle stages.

During the **mining stage**, rapid changes in cavern pressure and stress redistribution can increase the likelihood of dilation and permeation. With σ_3 relatively low compared to P_f, the system becomes more susceptible to dilation and permeation. Simulation results (Figure 17) show P_f approaching σ_3 (> 0.9) near the cavern wall making permeation very likely to occur at the cavern wall. However, since the dilatant zone is minimal, any micro-fracturing that may occur is likely not noticeable as the corresponding salt will be washed out as the cavern expands. Thus, while hydraulic fracturing seems probable at the cavern, it is very unlikely to propagate further if the operator controls the cavern pressure according to current practice (Rokahr et al. 1998; Berest et al., 2020), as reflected in the simulations. Beyond 15 m offset, the model results (Figure 18) indicate a negligible likelihood of hydraulic fracturing.

During the **waiting period**, the cavern pressure stabilizes, and viscoelastic relaxation of the salt leads to gradual stress redistribution. While σ_3 gently increases over time, its relationship to P_f remains a critical factor in determining whether micro-fracturing or enhanced permeation occurs. This period often exhibits lower permeation potential provided the operator maintains cavern pressure control according to standard practice, as reflected in the simulations. Here, the P_f remains below 80% of σ_3, making hydraulic fracturing very unlikely, even at the cavern wall. However, during the pressure decrease at the end of the waiting period, the simulations indicate that σ_3 decreases rapidly, while pore pressure near the cavern wall declines more gradually, depending on local permeability. This increases Δp and temporarily raises the likelihood of permeation and hydraulic micro fracturing. That said, practical operator experience during workovers under halmostatic conditions shows that brine tends to flow out of the well at surface. This suggests that brine warming, and creep convergence are dominant processes, outweighing potential permeation or small-scale hydraulic fracturing under these conditions.

During **abandonment**, equilibrium cavern pressure becomes the dominant factor. A high equilibrium pressure increases σ_3, enhancing confinement of the salt host rock and generally reducing the risk of hydraulic fracturing. However, localized stress concentrations near the cavern walls may still pose a risk if P_f exceeds critical thresholds. The evolution of σ_3 relative to P_f throughout this stage is crucial for assessing long-term stability and fracture risk. Multiple superimposed phenomena influence this phase. In the late abandonment, permeation plays a role and causing some deviations from the general decreasing trend through viscoelastic relaxation (Figure 19).

At the start of abandonment, as cavern pressure rises, Δp generally decreases. However, reversals of Δp are observed in the upper part of many caverns, where Δp temporarily increases before relaxing over time. This reversal is linked to a shift in the orientation of the least compressive principal stress (σ_3). When cavern pressure is sufficiently low, σ_3 aligns with the normal stress at the cavern wall. As cavern pressure increases, σ_1 reorients to align with the cavern normal stress, while σ_3 shifts to align with the tangential stress at the cavern wall.

This phenomenon is also evident in Figure 20 and Figure 21, which provide an overview of how Δp evolves across the entire cavern field at 0 meters and 25 meters offset from the cavern wall. The results indicate that the conditions stabilize with increasing offset from the cavern wall suggesting that effects of stress reorientation and Δp fluctuations diminish further from the caverns. Overall, P_f remains below ~80% of σ_3, at the cavern wall, suggesting stable conditions. This assessment aligns with earlier findings shown in the final report (e.g., p.212, Fig. 172, Abandonment of solution mining cavern field Zuidwending, The Netherlands – an integrated, multiscale investigation, version 240411), which states that in the late abandonment, the orientation of the maximum principal stress in the cavern roofs is oriented normal to the cavern walls. This orientation suggests a preferential sub-horizontal fracture propagation between caverns.

Note that the evaluating the principal stress at the cavern wall involves an extrapolation step, introducing some uncertainty in predicting the exact conditions at the cavern wall. Therefore, while the assessment at 0 m offset suggests that no microfracturing occurs, we adopt a conservative assumption and consider the likelihood of hydraulic fracture initiation at the cavern wall as probable or likely. However, given the Factor of Safety (FOS) conditions, and the stress orientation beyond 15 m offset, it is very unlikely that a large-scale subvertical fracture propagate into the formation.

To illustrate how the system stabilizes with increasing offset from the cavern wall, we refer to Figure 19, which provides insights into how the system stabilizes (e.g., for ZW-6) with larger distance from the wall. As the distance from the cavern wall increases, the pore pressure must overcome progressively larger least compressive stresses to induce permeation or hydraulic fracturing. However, with the onset of a hydraulic fracturing at the cavern wall, the coupled system locally alters the stress state, meaning hydraulic (micro) fracturing is probable to occur at the cavern wall. Small-scale propagating hydraulic fractures could occasionally occur for close distances from the cavern wall (<15 m) Nevertheless, the stress state near the cavern field does not favour the development of a massive hydraulic fracture.

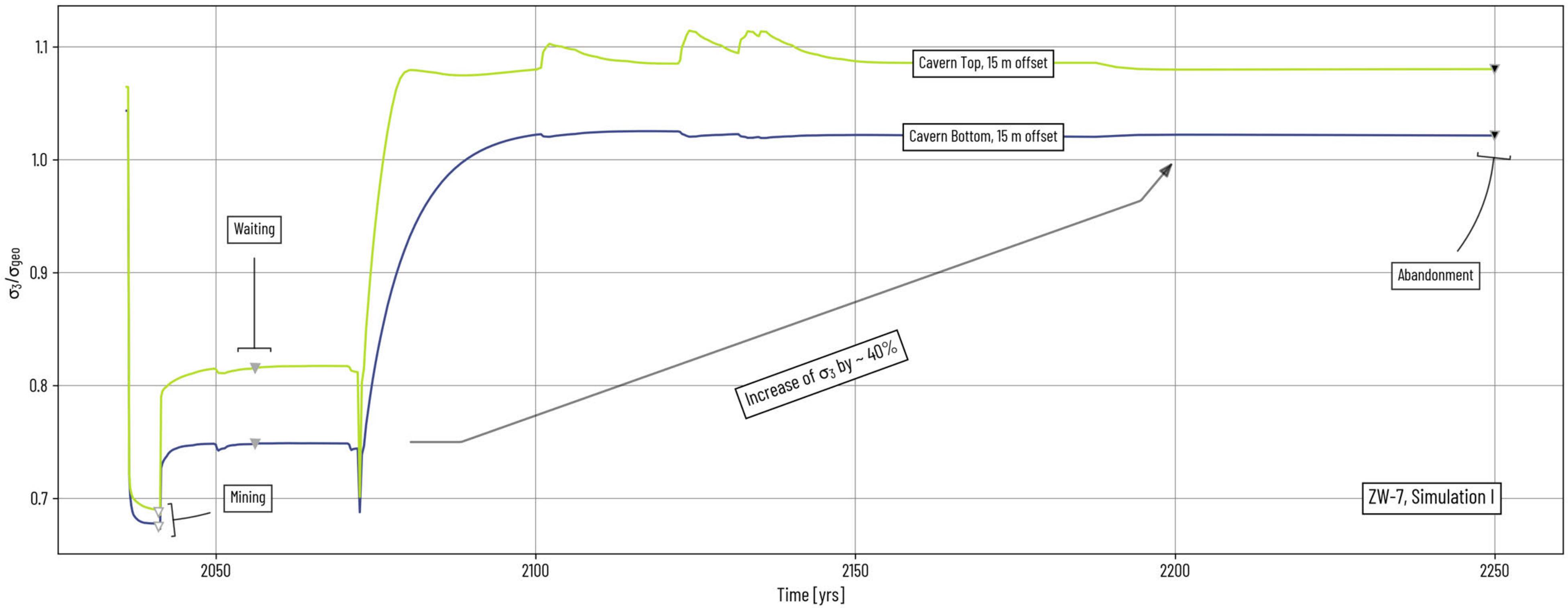

Figure 16. Evolution of σ_3 relative to σ_{geo}, for top and bottom of cavern ZW-7, with 15 m offset from cavern wall. Similarly, P_f values are extracted for all caverns. σ_3 increases by 40% from waiting to abandonment.

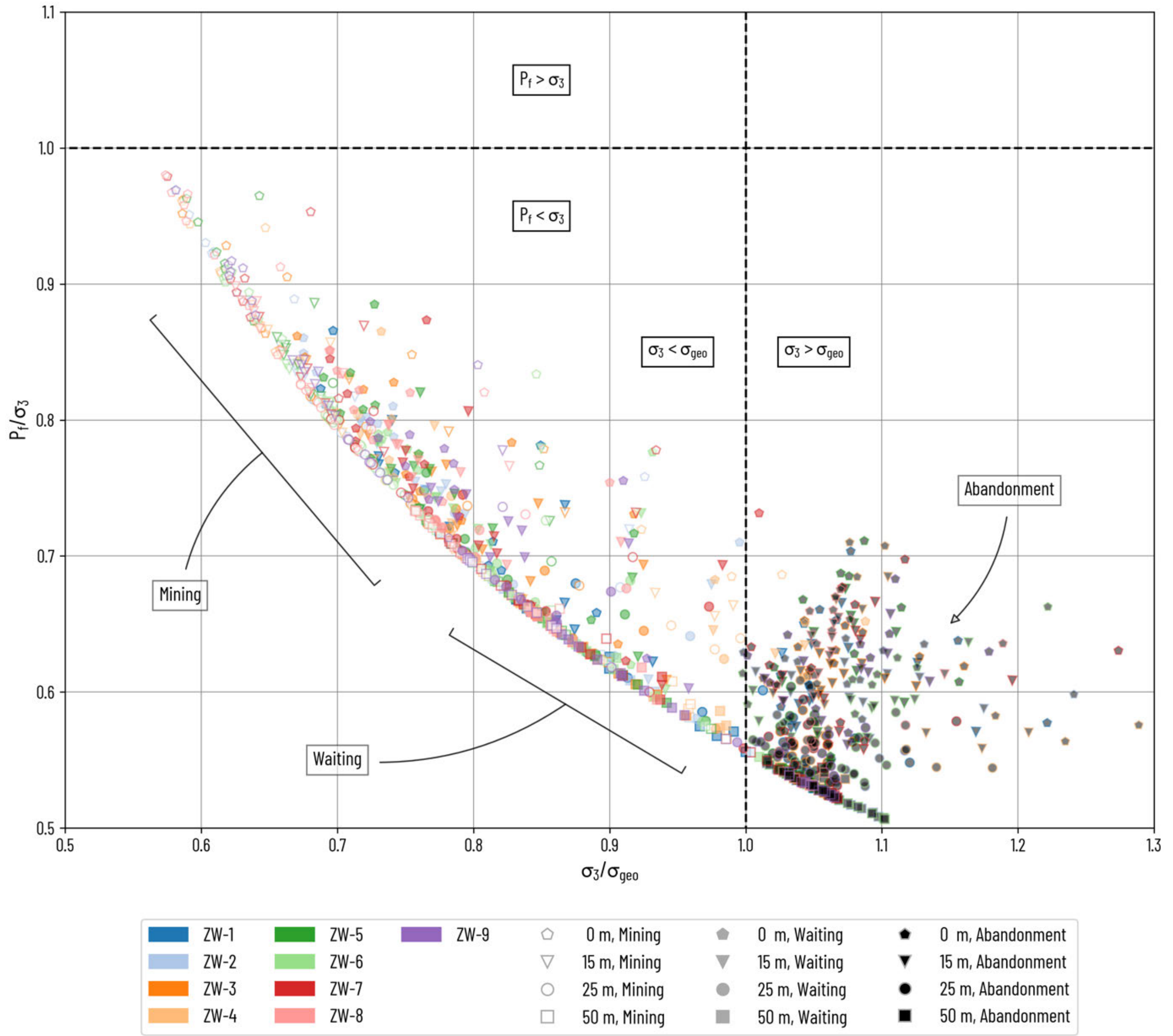

Figure 17. Summary of query results for entire cavern field, demonstrating that σ_3 is higher than σ_{geo} in abandonment, but lower than σ_{geo} during the waiting period. Only at close distances from cavern walls (e.g. pentagons: 0 m, triangles: 15 m), P_f is slightly increased, but only 70% max. of σ_3 at most. Further away, P_f is a function of σ_3 (squares: 50 m offset).

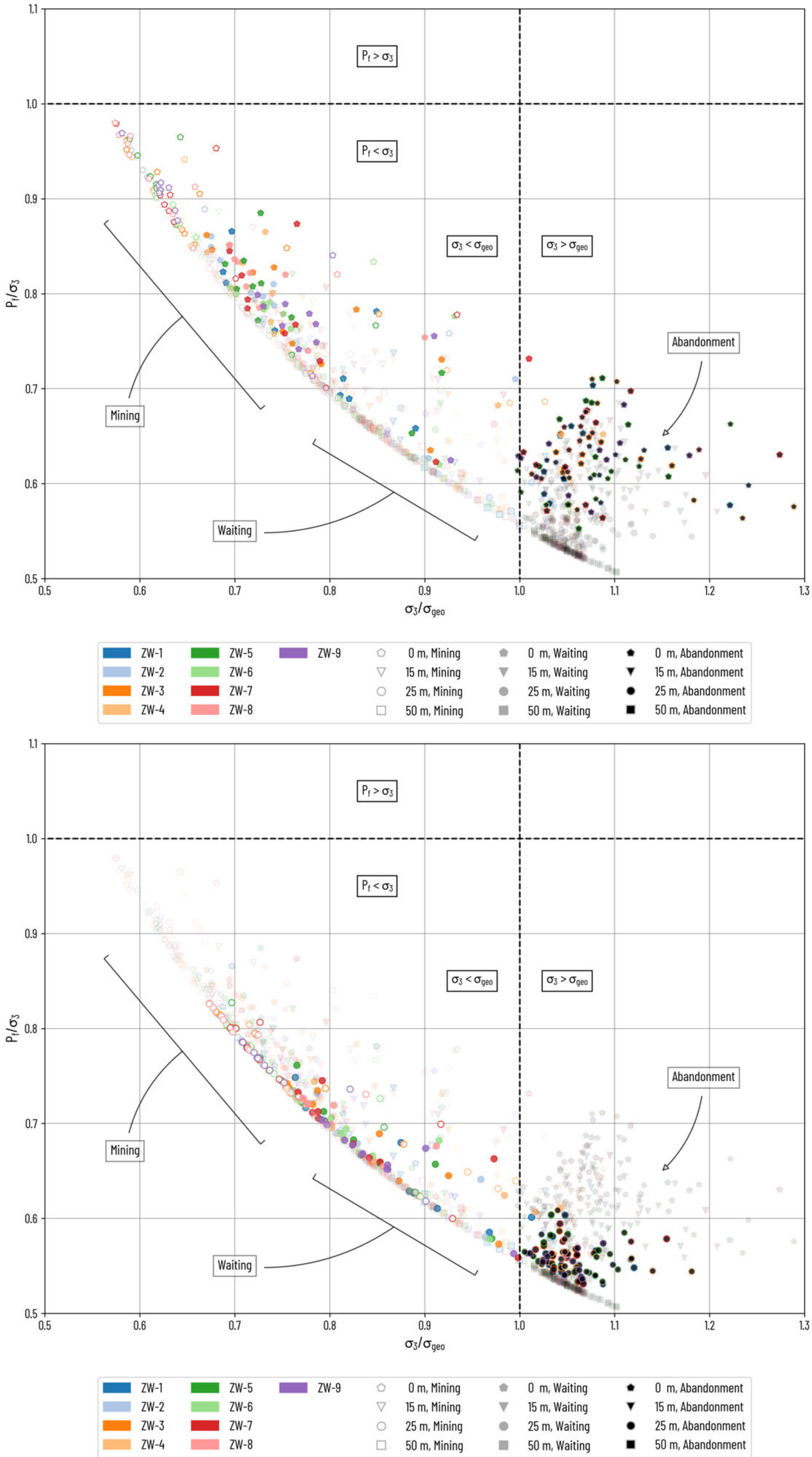

Figure 18. As Figure 17 but highlighting characteristic values obtained at the cavern wall (top), and in 25 m offset from the cavern wall (bottom). Versions of this figure highlighting 15 m and 50 m offsets are provided as appendix.

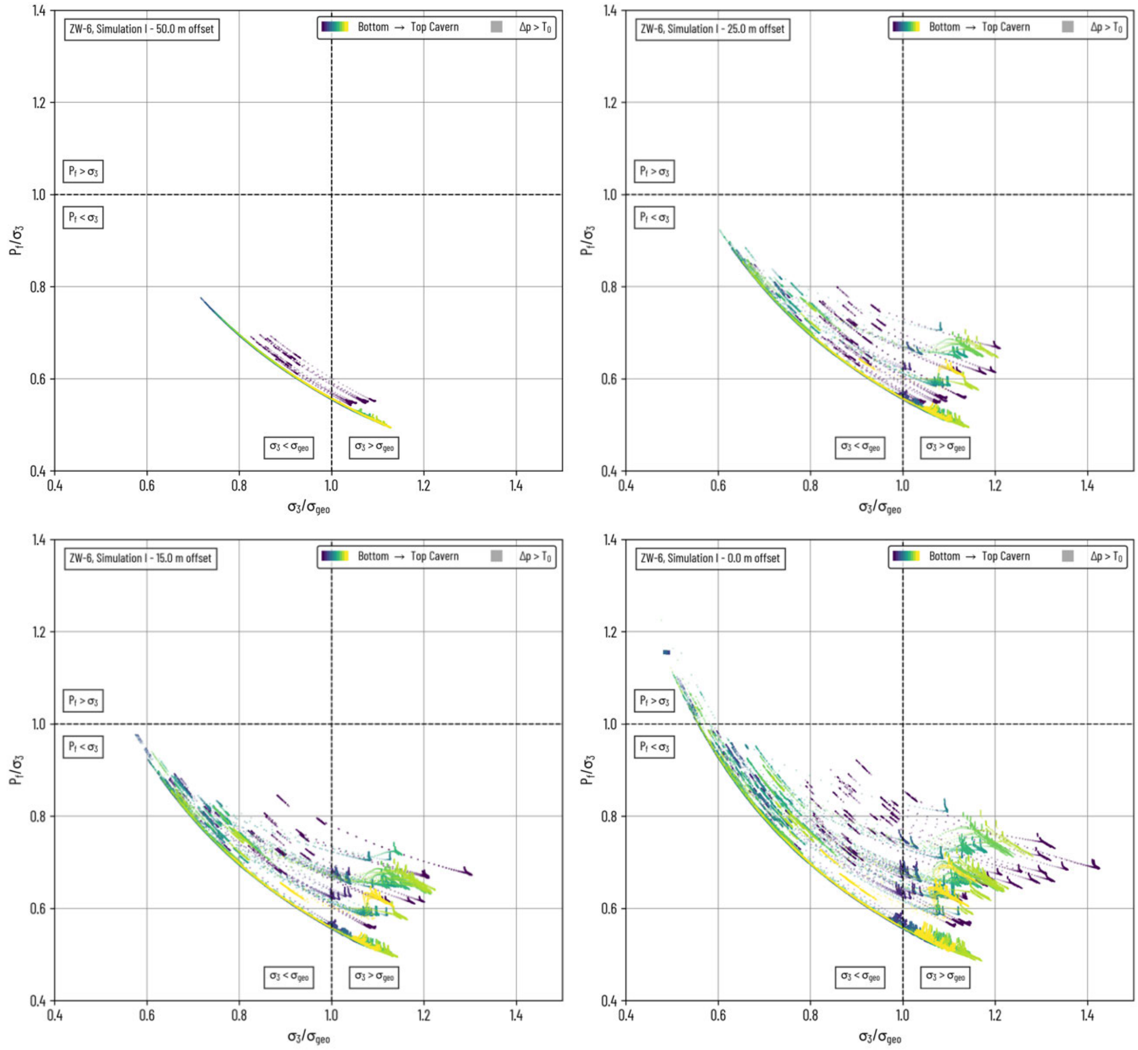

Figure 19. As Figure 17 but evaluated for the continuous cavern life cycle (here ZW-6) at various depths relative to the cavern height and at different offset distances. In all offset cases, the pore pressure remains below the least compressive stress. The situation at the cavern wall is linearly extrapolated due to resolution limitation of the dome-scale simulations. Nevertheless, at some location (square markers) we obtain $\Delta p > T_0$ in the close vicinity of the cavern wall and localized fracture onsets can thus not be excluded.

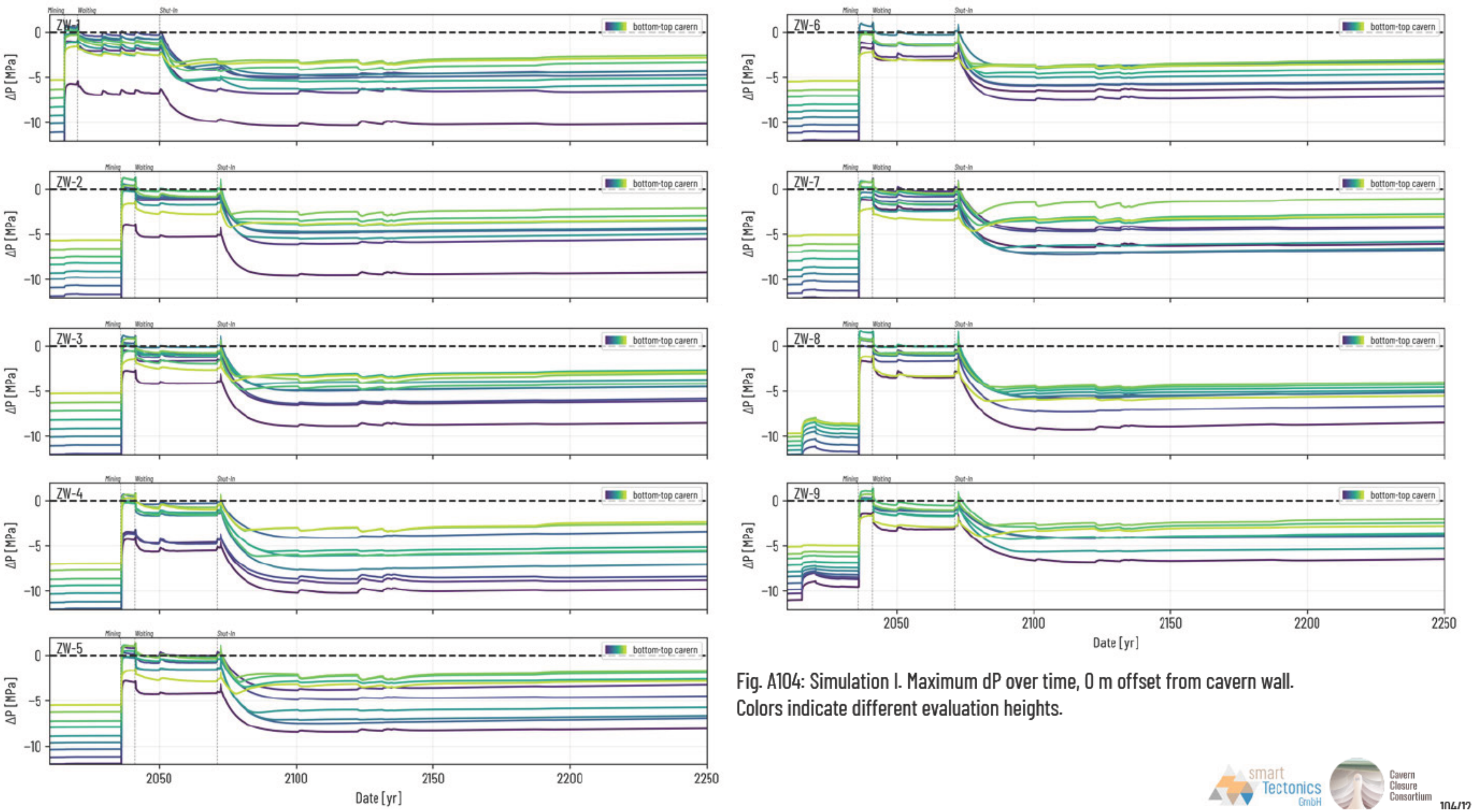

Figure 20. The evolution of the maximum Δp (at cavern wall) is shown throughout the full cavern lifecycle at the cavern wall across specific depth levels. While conditions for permeation onset are met during the waiting period up to the start of abandonment, the magnitude of Δp decreases over time during the abandonment phase. A high-resolution version of this figure is provided as appendix.

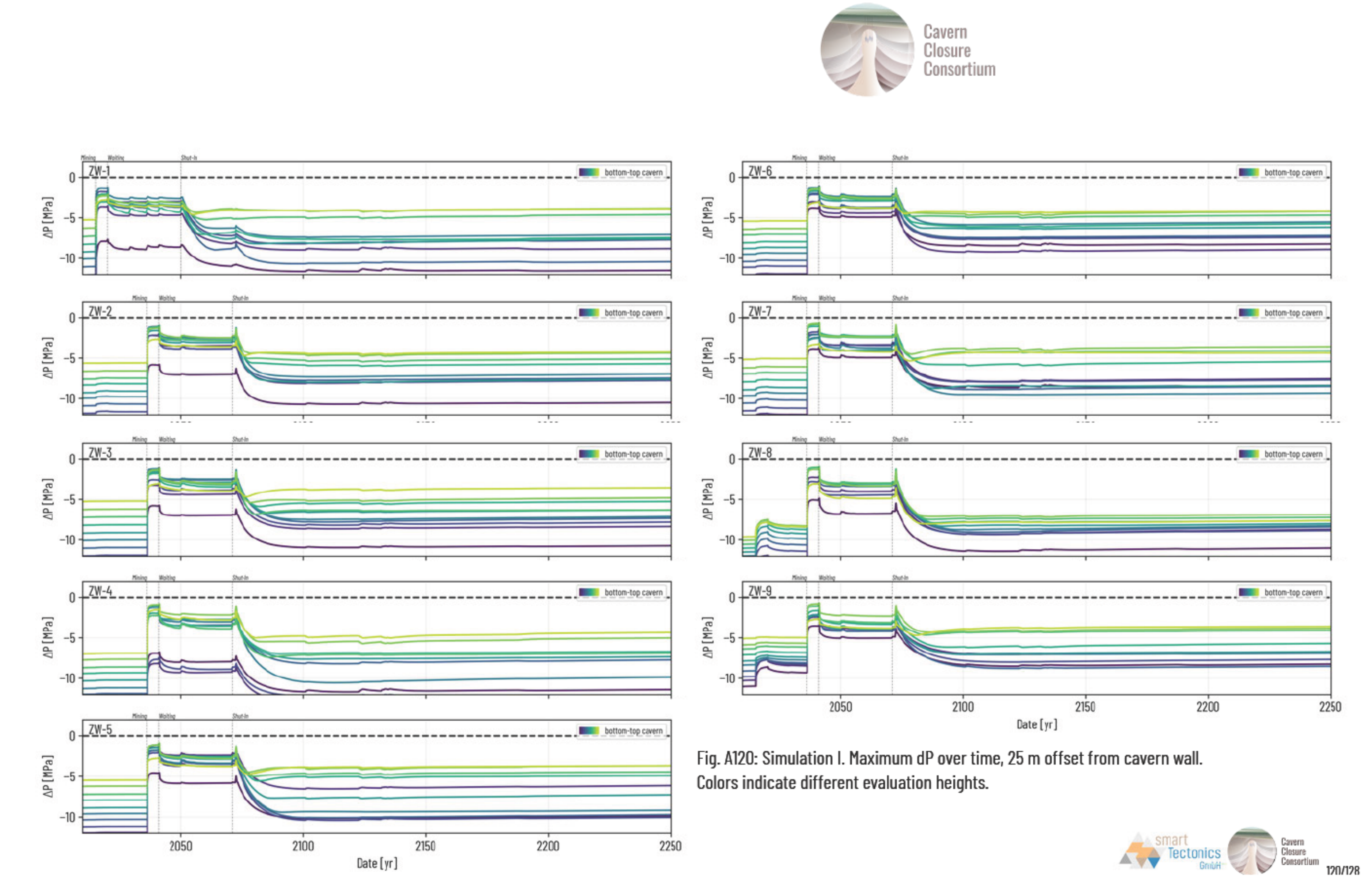

Figure 21. The evolution of the maximum Δp (25 m offset from cavern wall) is shown throughout the full cavern lifecycle at the cavern wall across specific depth levels. While conditions for permeation onset are met during the waiting period up to the start of abandonment, the magnitude of Δp decreases over time during the abandonment phase. A high-resolution version of this figure is provided as appendix.

3.7 Consequences of opening a fracture

In the event of a fracture opening, the brine escaping from the cavern through the fracture will reduce the rate of pressure increase in the cavern. Unlike a fracture test in an openhole where it is easy to maintain the pumping rate to keep the fracture open, this is less obvious at cavern scale where pressure increase rates are much lower because instead of pumping pressure is only increased by slow brine warming and (at relatively high pressures) slow creep convergence. The micro-fracking process in a cavern after abandonment is very probably much smoother than what can be observed during a standard fracture test. It is highly likely that, when cavern pressure increases, the number and length of the micro-fractures increase. It is possible that, after some time, localization takes place: most micro-fractures stop growing, a small number of the micro-fractures keep growing (their aperture and their length increase), leading to the formation of “fractures”.

The very unlikely opening of a fracture of significant size would have the effect of increasing the compressibility of the cavern, as was observed during the Etzel abandonment test (Staudtmeister & Rokahr, 1994; Djizanne et al., 2012). This increase in compressibility will have the effect of slowing the increase in pressure, which is the driving force behind fracture development.

It should also be noted that the development of a fracture requires a certain amount of energy, which is difficult to assess at this stage of the study, which again is an obstacle to the development of the fracture.

In the worst-case scenario, if a hydraulic connection is established between a cavern and the overburden, the flowrate through this fracture can be estimated. Neglecting friction, a very rough estimate of the velocity v of the brine arriving in the overburden can be made using Bernouilli's principle:

$$gZ_{cav} + \frac{P_{cav}}{\rho_b} = \frac{v^2}{2} + gZ_{over} + \frac{P_{over}}{\rho_b} \quad (1)$$

Where ρ_b is saturated brine density; Z_{cav} and Z_{over} are respectively the depths of the cavern roof and the base of the overburden; P_{cav} and P_{over} are respectively the pressures at the cavern roof and at the base of the overburden. The velocity of the brine is then expressed:

$$v = \sqrt{2\left[\frac{P_{cav} - P_{over}}{\rho_b} - g\left(Z_{cav} - Z_{over}\right)\right]} \quad (2)$$

Assuming a hydrostatic pressure in the overburden, a maximum pressure gradient of the order of $\rho_{max} g = 0.3$ bar/m in the cavern (from the numerical calculations), and ΔZ is the thickness salt roof, we obtain

$$v = \sqrt{2g\left[\left(\frac{\rho_{max} - \rho_w}{\rho_b}\right)Z_{cav} - \left(\frac{\rho_b - \rho_w}{\rho_b}\right)\Delta Z\right]} \quad (3)$$

When considering for instance the cavern ZW-9, one of the closest to the overburden, $Z_{cav} = 470$ m, and the thickness of the salt roof is $\Delta Z = 200$ m, then the velocity would be in the order of 123 m/s. Assuming a 1 cm² cross-section of the fracture, this would provide a 1060 m³/day flowrate.

In the case of the ZW-1 cavern, which is closest to the side of the dome, we can imagine a fracture developing more horizontally, in which case equation (1) would become:

$$v = \sqrt{2\frac{P_{cav} - P_{over}}{\rho_b}} = \sqrt{2g\left(\frac{\rho_{max} - \rho_w}{\rho_b}\right)Z_{cav}} \tag{4}$$

and with $Z_{cav} = 475$ m for ZW-1, the velocity would be in the order of 127 m/s. Assuming a 1 cm² cross-section of the fracture, this would provide a 1100 m³/day flowrate.

Clearly, this extremely simplistic model greatly overestimates the flow rate through the fracture, as there will be a huge loss of head, and the average cross-sectional area of the fracture will probably be much smaller. As the compressibility of caverns is of the order of $\beta V =$100 to 200 m³ per bar, any leakage rate as mentioned above and up to the volumes as mentioned in the scenarios below, would thus cause the cavern pressure to drop and stop the fracture and leak.

Scenarios after opening a fracture

There are a number of possible scenarios following the opening of a fracture.

- A realistic scenario based on Etzel test would be that the cavern pressure will drop from a gradient in the order of ~0.225 bar/m to a gradient of ~0.220 bar/m. Translated to ZW-5 (the cavern with the largest compressibility, in the order of $\beta V = 220$ m³/bar,), this would be a drop of ~2,5 bar and a corresponding volume of ~540 m³ leaving the cavern and entering the surrounding rock salt.

- We can imagine a more conservative scenario in which a fracture opens when the cavern pressure exceed the geostatic pressure by an amount corresponding to the tensile strength T_0, which is of the order of 1.5 MPa. The flow of brine out of the cavern through this fracture will tend to reduce the pressure in the cavern. If we assume that the fracture closes when the cavern pressure falls back to geostatic pressure, then the leakage volume would be

$$\Delta V = \beta V \times T_0 \tag{5}$$

  ZW-5 is the cavern with the largest compressibility, in the order of $\beta V = 220$ m³/bar, and the leakage leaving the cavern and entering the surrounding rock salt would be in the order of 3300 m³ for this cavern.

- If we assume in a worst case third scenario that the fracture opens at a pressure gradient of $\rho_{max} g = 0.3$ bar/m and closes at a pressure close to the geostatic pressure, then the leakage volume would be:

$$\Delta V' = \beta V \left(\rho_{max} - \rho_{geo}\right) g Z_{cav} \tag{6}$$

  where $\rho_{geo} \approx 2200$ kg/m³ is the average density of the rocks above the cavern.

  Then the leakage volume leaving the cavern and entering the surrounding rock salt would be:

$$\Delta V' = 170 \times \left(0.3 - 0.22\right) \times 630 \approx 8600 \text{ m}^3$$

Note that all the former volumes are based on the planned end volumes of the caverns.

3.8 Conclusions on the likelihood of hydraulic fracturing

Before abandonment, pressure decreases to halmostatic conditions may cause some damage in the first few meters around the cavern wall, leading to localized dilation and permeation. However, the likelihood of hydraulic fractures propagating beyond 15 meters remains negligible.

After abandonment, permeation is expected, particularly near the cavern wall and roof. In the first months to years following abandonment, when pressure increases at a relatively high rate, small-scale hydraulic fracturing could also occur in these areas. Nevertheless, the propagation of hydraulic fractures beyond 15 meters remains highly unlikely.

In the long term, as stress differences decrease and brine warming decreases, permeation may continue, but the likelihood of hydraulic fracture formation diminishes further. While hydraulic fractures cannot be completely ruled out, the possibility of a large subvertical fracture propagating beyond 15 meters from the cavern wall is extremely low.

After considering several scenarios and the planned end volume of a representative cavern, it appears that the volume of brine that could escape from the cavern to surrounding layers through one of several fractures remains very limited, ranging from 540 m^3 to 8,600 m^3.

Table 1. Summary of different evaluation quantities, findings from simulations, and observations used to interpret the likelihood of hydraulic fractures from abandoned caverns. * Permeation denotes non-linear, pressure driven permeability

Cavern life-cycle phase	**Evaluation criteria**	**Evaluation results**	**Likelihood based on simulation results**
Operation & Waiting	Dilation $FOS \leq 1$	$FOS \leq 1$ for some cases during mining. During waiting 1<FOS <2 at the cavern wall. With offset from cavern wall FOS increases. During the pressure decrease at the end of the waiting period (cementing) FOS temporarily decreases. However, even during this short period the FOS remains above 1.	Dilation is likely to occur at the cavern wall. When assessing against the very conservative DeVries criterion, it could also occur at 15 m offset from the cavern wall, but not beyond 25 m. If there was a minimal dilatant zone, it is likely not noticeable as it will be washed out as the cavern expands. Thus, it is important to emphasize that it would not affect cavern integrity.
	Permeation $P_f \geq \sigma_3$ $\Delta p \geq 0$	Permeation occurs at the cavern wall, during mining and also during waiting at a lower pressure.	Permeation is very likely to occur at the cavern wall and in close offsets (<15 m) from the cavern wall. The likelihood of permeation to occur at offsets > 25 m from the cavern wall is considered negligible provided the operator manages the cavern pressure along the current practice (as has been included in the simulations).
	Fracturing $P_f > \sigma_3 + T_0$ $\Delta p \geq T_0$	At halmostatic conditions during mining, the simulation results predict $P_f > \sigma_3 + T_0$ at the cavern wall-for some caverns. This specifically refers to the pressure decrease at the end of the waiting period (cementing) which temporarily increases Δp for a short duration and may exceed T_0 in some localized areas at the cavern wall.	Small-scale hydraulic (micro) fracturing is probable to occur at the cavern wall during halmostatic conditions. Given the FOS conditions, and the stress orientation, the likelihood of propagating hydraulic fractures beyond 15 meters from the cavern wall at halmostatic conditions is negligible provided the operator manages the cavern pressure along the current practice (as has been included in the simulations). The practical experience of the operator shows that during workovers at halmostatic conditions, brine tends to flow out of the well at surface, indicating that brine warming and creep convergence are dominant over

			any possible permeation or small-scale hydraulic fracturing under these conditions.
After P&A < 5 years after shut-in	Dilation $FOS \leq 1$	As soon as the cavern is abandoned, FOS increases with cavern pressure. FOS increases quickly after plug and abandonment and within 5 years after plug and abandonment FOS is larger than 2. It also increases with further offset from cavern wall.	Even when assessing against the very conservative DeVries criterion, the likelihood of dilation to occur is negligible after P&A.
	Permeation $P_f \geq \sigma_3$ $\Delta p \geq 0$	Correlated with FOS, Δp increases at the cavern wall at halmostatic conditions during shut-in process. Afterwards Δp is decreasing. At >=25 m offset from the cavern wall, there is no indication that permeation occurs.	Permeation is very likely to occur at the cavern wall. Permeation is probable also at 15 m offset from the cavern wall, but it becomes unlikely with further offset and with increasing pressure.
	Fracturing $P_f > \sigma_3 + T_0$ $\Delta p \geq T_0$	At halmostatic conditions during the shut-in process, the simulation results predict $P_f > \sigma_3 + T_0$ at the cavern wall for some caverns. After shut-in: while for the cavern wall it cannot be excluded that (micro) fractures occur locally below the resolution limit, the dome-scale simulation results predict $P_f < \sigma_3 + T_0$ during the abandonment phase.	Hydraulic (micro) fracturing is probable to occur at the cavern wall. Small-scale propagating hydraulic fractures could occasionally occur for close distances from the cavern wall (<15 m). This agrees with the Etzel findings that (small-scale) hydraulic fractures are occurring close to the cavern wall during a fast pressure increase. To put it into perspective, at the Etzel test the pressure increase in the second and third pressurization step was 0.36 bar/day and 0.24 bar/day respectively. In the Zuidwending simulation it is maximum 0.05 bar/day. Given the FOS conditions, and the stress orientation, also in +15 m offset from the cavern wall, it is very unlikely that a massive subvertical fracture propagates.
Abandonment >> 5 years after shut-in	Dilation $FOS \leq 1$	Dilation criterion is usually not met.	When assessing against the very conservative DeVries criterion, dilation is unlikely to occur at the cavern wall. When FOS increases with cavern pressure the likelihood of dilation to occur at +15 m offset from the cavern wall is negligible.

	Permeation $P_f \geq \sigma_3$ $\Delta p \geq 0$	Permeation is expected to occur at certain locations in the cavern wall or roof.	Permeation is expected to occur in the upper part of the caverns. Over time, permeation is very likely to occur in distances >= 25 m from the cavern wall
	Fracturing $P_f > \sigma_3 + T_0$ $\Delta p \geq T_0$	While for the cavern wall it cannot be excluded that (micro) fractures occur locally below the resolution limit, the simulation results predict $P_f < \sigma_3 + T_0$ during the long term abandonment phase.	Hydraulic (micro) fracturing could occasionally occur at the cavern wall. Small-scale propagating hydraulic fractures have a remote likelihood to occur for close distances from the cavern wall (<15 m). This agrees with the Etzel findings that (small-scale) hydraulic fractures are occurring close to the cavern wall at sufficiently elevated pressures. Given the FOS conditions, and the stress orientation, also in +15 m offset from the cavern wall, it is very unlikely that a massive subvertical fracture propagates beyond that point.

4 2D modelling of the abandonment of ZW-3 cavern after end of mining in 2025 compared to end of mining in 2040

4.1 Summary

In the April 2024 report, we carried out a sensitivity study on the behaviour of the ZW-3 cavern because it is representative as it is the highest cavern of the group ZW-2 to ZW-9. Therefore, additional 2D calculations were performed to check whether or not it was necessary to perform more 3D simulations.

The former calculations were based on the planned end situation; i.e., end of mining of this cavern would end in 2040 (2035 in Nobian permit application). Where this document mentions 2040 to stay in line with the original CCC Zuidwending report (CCC, 2024), the same end shape and volume is meant as applied for 2035 in the Nobian extraction plan. Additional calculations are presented below to compare this initial end of mining scenario with an early shutdown of cavern mining at the end of 2025. The main conclusions are as follows:

- ✓ The likelihood of hydraulic fracturing is similar between the 2025 and 2040 case.

- ✓ In the event of hydraulic fracturing, it is estimated that the volume of brine expelled into the surrounding area will be approximately 25% less in the 2025 case than in the 2040 case, resulting in a maximum estimated volume of ~6400 m^3, a realistic case volume of ~2500 m^3 and an optimistic case volume of ~400 m^3, instead of ~8600 m^3, ~3300 m^3 and ~540 m^3 respectively.

4.2 Calculation assumptions

Figure 22 shows a comparison of the 2D axisymmetric shapes of the ZW-3 cavern at the end of mining, depending on whether it stops in 2025 or 2040. In the first case, the volume at the end of mining is 5 million m^3, while in the second it is 6.3 million m^3.

Of the 12 configurations studied in the sensitivity analysis in the 2024 report (CCC, April 2024), the focus here is on case #11 (Table 2) because this case corresponds to the reference case in this report, in particular with abandonment when the temperature difference to be absorbed is only about 5°C, with the “expected” creep for the pressure solution mechanism, without threshold, and a permeation scenario of type D used as base case in the CCC report.

For the coupling between permeability and effective tangential stress, scenario D is considered, the values of which are given in Figure 23.

It is assumed that mining is shut down at the end of 2025 and that there is a 24-year waiting period before definitive closure. It is also assumed that the temperature of the brine in the cavern is 24°C at the end of mining. This value is based on practical experience in the field, and also on ZW-1 which is was taken out of production recently and currently in the waiting phase.

The Figure 24 shows the increase in temperature in the cavern after the end of mining. The Figure 25 shows the evolution of the temperature difference that needs to be absorbed to reach thermal equilibrium in the cavern.

The Figure 26 shows the pressure evolution at the cavern roof at a depth of 474 m. The pressure reached a maximum of 125.4 bar in 2056, 6 years after abandonment. This pressure corresponds to a gradient of 0.264 bar/m.

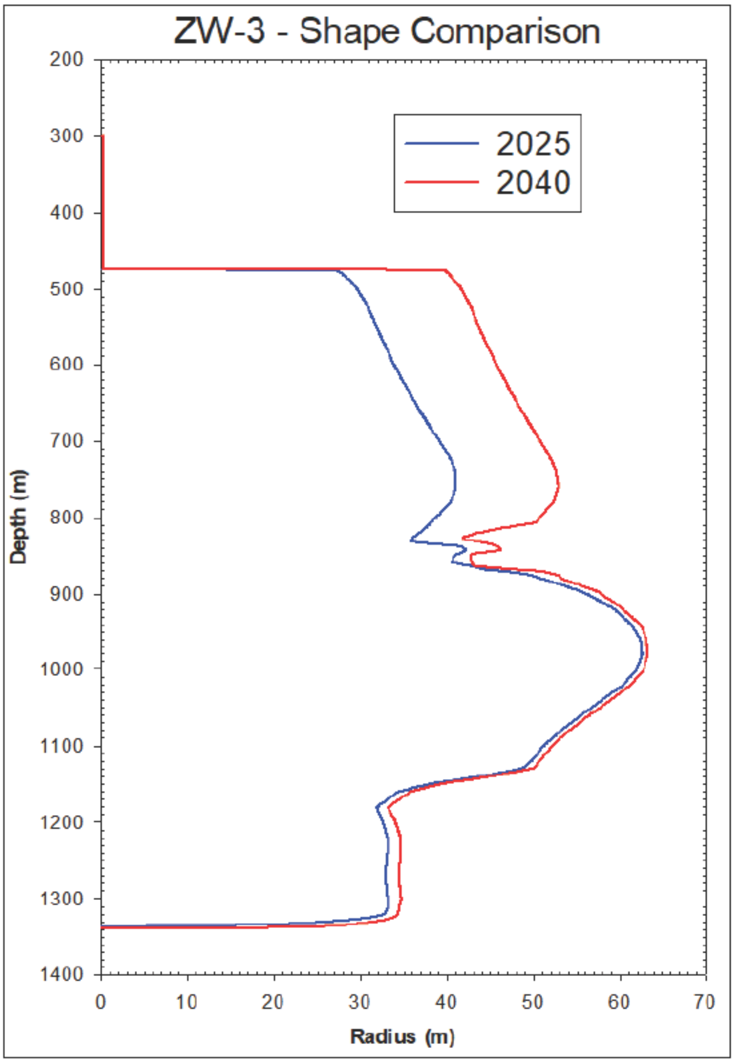

Figure 22. Comparison of the shapes of 2025 and 2040 superimposed on each other.

Table 2. Table for the sensitivity analysis of ZW-3 (CCC April 2024 report).

Case	Temperature gap (°C)	Waiting time (years)	Creep Scenario	Permeation behaviour scenario	Threshold for pressure solution (MPa)
#01	12.7	0	Expected	D	0
#02	3	50	Expected	D	0
#03	5	24	Expected	C	0
#04	5	24	Conservative	C	0
#05	3	50	Expected	A	0
#06	3	50	Expected	B	0
#07	3	50	Expected	C	0
#08	3	50	Expected	E	0
#09	3	50	Conservative	D	0
#10	3	50	Kristalbrocken	D	0
#11	5	24	Expected	D	0
#12	3	50	Expected	D	0.07

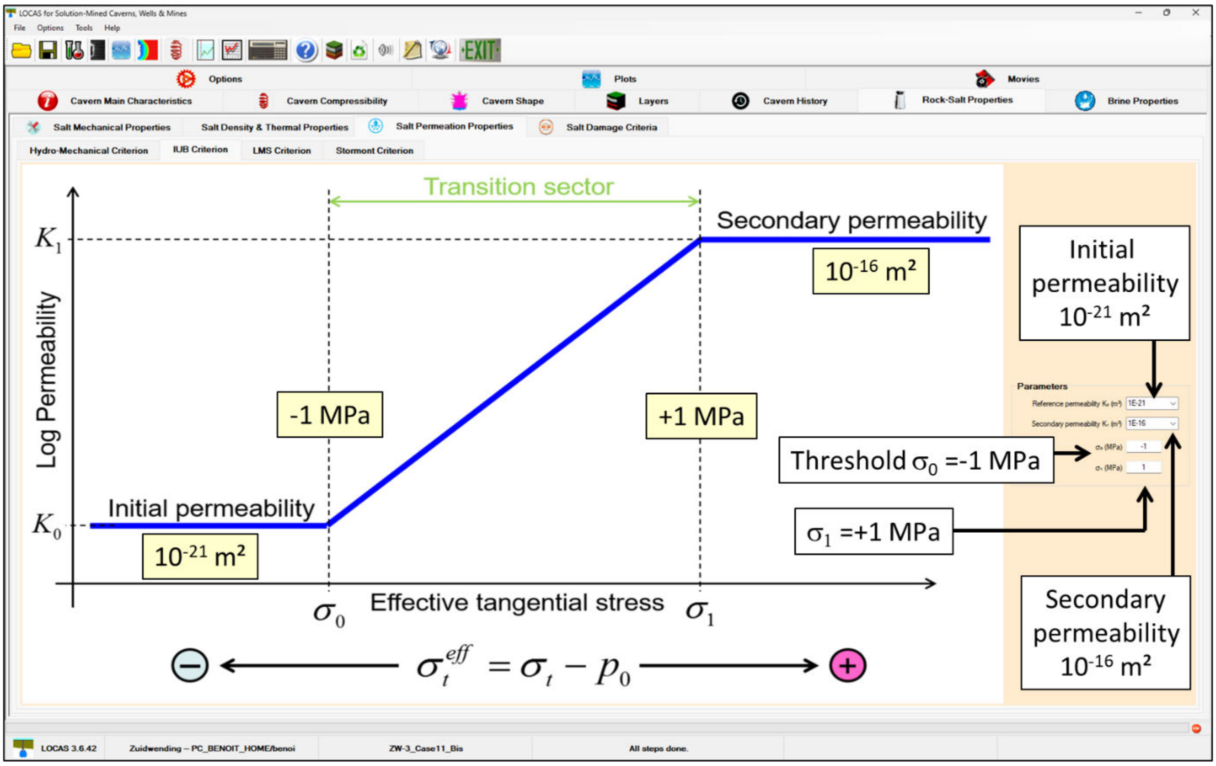

Figure 23. Considered coupling between permeability and effective tangential stress.

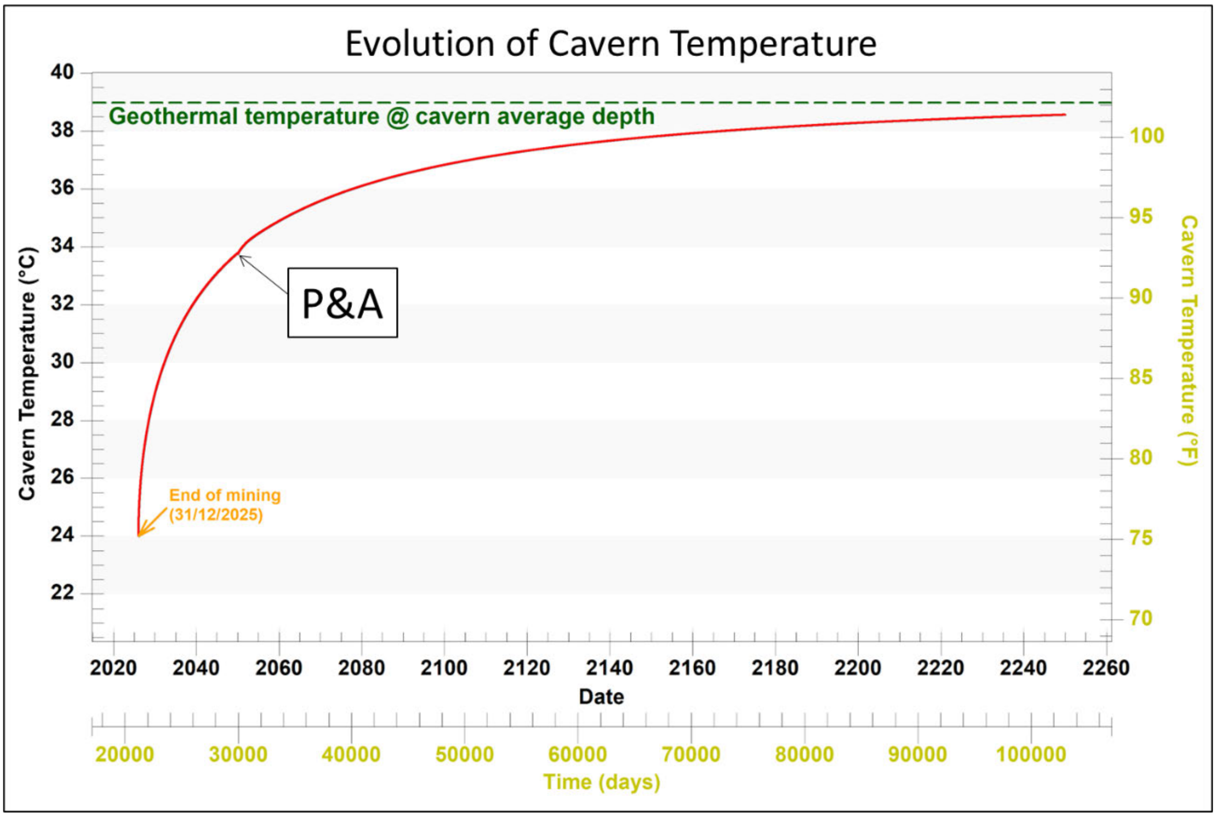

Figure 24. Evolution of cavern temperature.

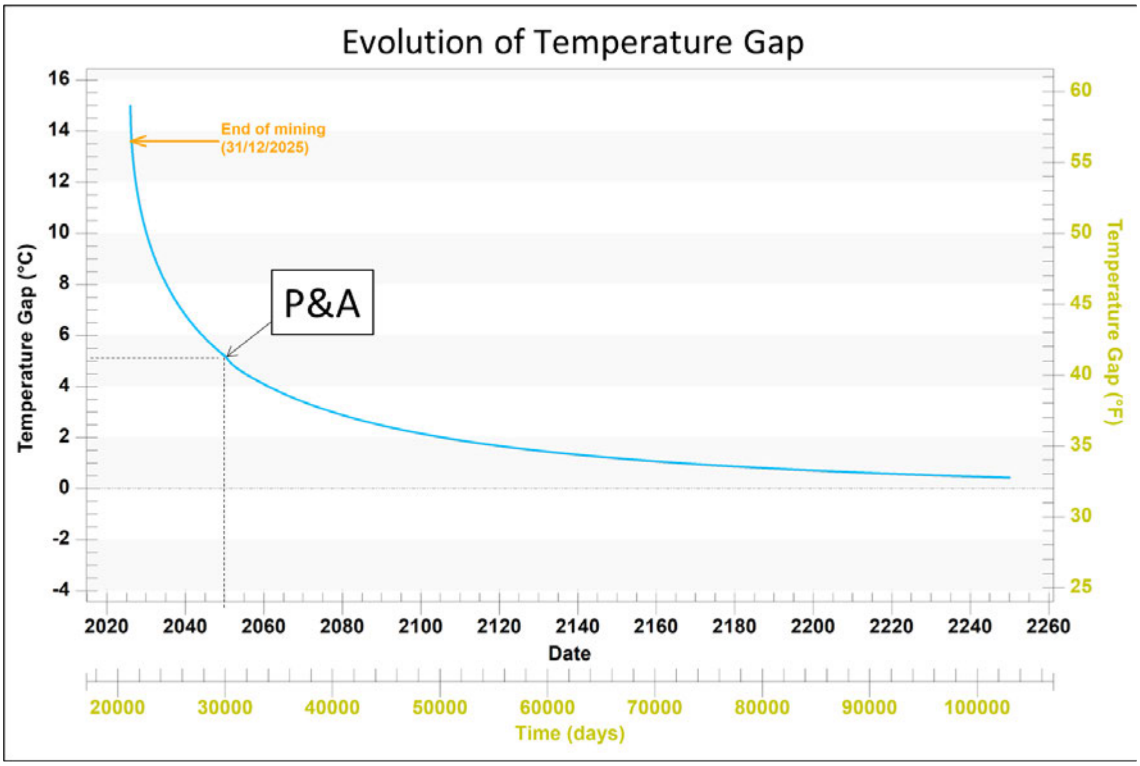

Figure 25. Evolution of the temperature gap to be resorbed.

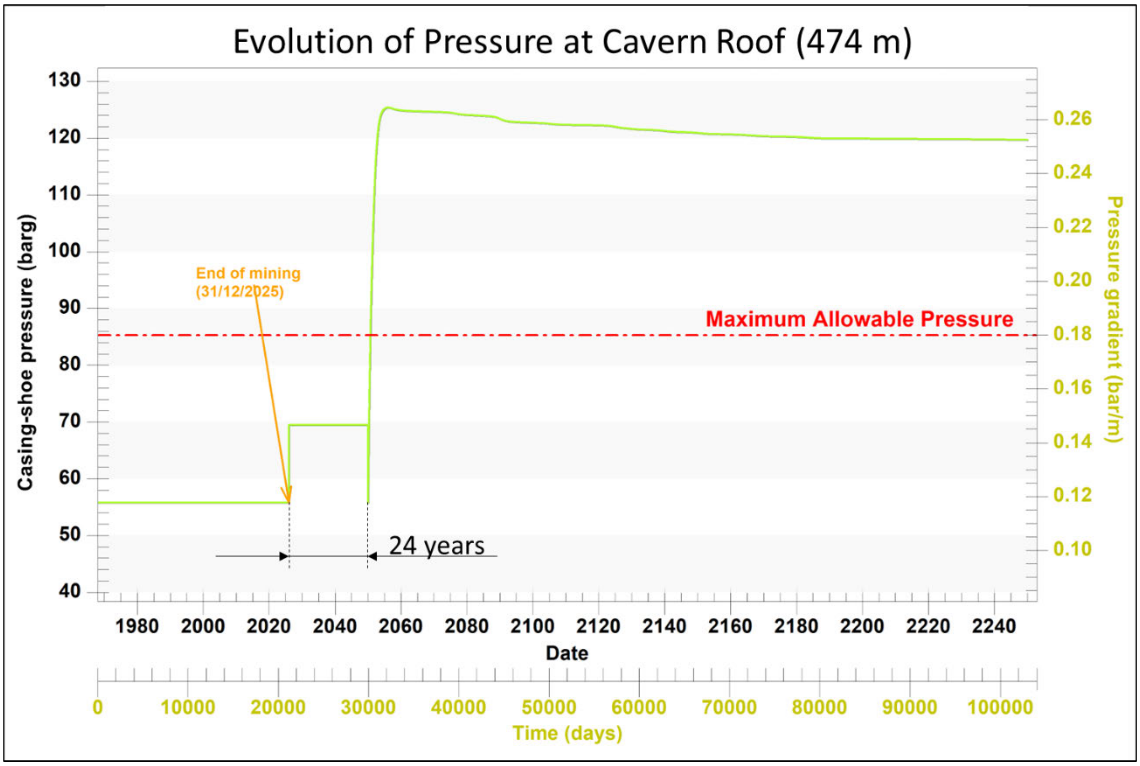

Figure 26. Evolution of pressure at cavern roof.

4.3 Comparison of results

Figure 27 shows a comparison of temperature changes in the cavern depending on whether mining stops in 2025 or 2040. Given that in the first case the cavern is a little smaller (the volume ratio is 1.26), the compressibilities of caverns are in the ratio of volumes, so the smaller cavern is stiffer, additionally there is less brine, and it heats up a little faster. As the characteristic time for warming depends on the volume at two-thirds power, it can be estimated that warming will be 16% faster at the time of closure if mining is finished in 2025. This is one of the reasons why pressure rises slightly faster after closure in the case of mining shut down in 2025 (Figure 28). The faster heating corresponds to a slightly faster increase in pressure due to the thermal expansion of the brine in the cavern. However, the pressure increases in the two caverns are very similar because cavern convergence is the main phenomenon leading to pressure increase. The pressure reaches a slightly higher value in the case of an early shutdown because the stresses have had less time to redistribute and the threshold for increasing permeability is reached later. This effect has been initially described in Karimi-Jafari et al. (2006).

Figure 29 and Figure 30 compare convergence and permeation rate respectively. The differences are small. In the long term, the loss of volume is the same, but, as cavern volume is different, the relative convergence rate is faster at the time of abandonment if mining is finished in 2025. This is due to the relaxation of the constraints, which tends to reduce the rate of convergence over time. Figure 31 compares the cumulated permeation. The differences are also small.

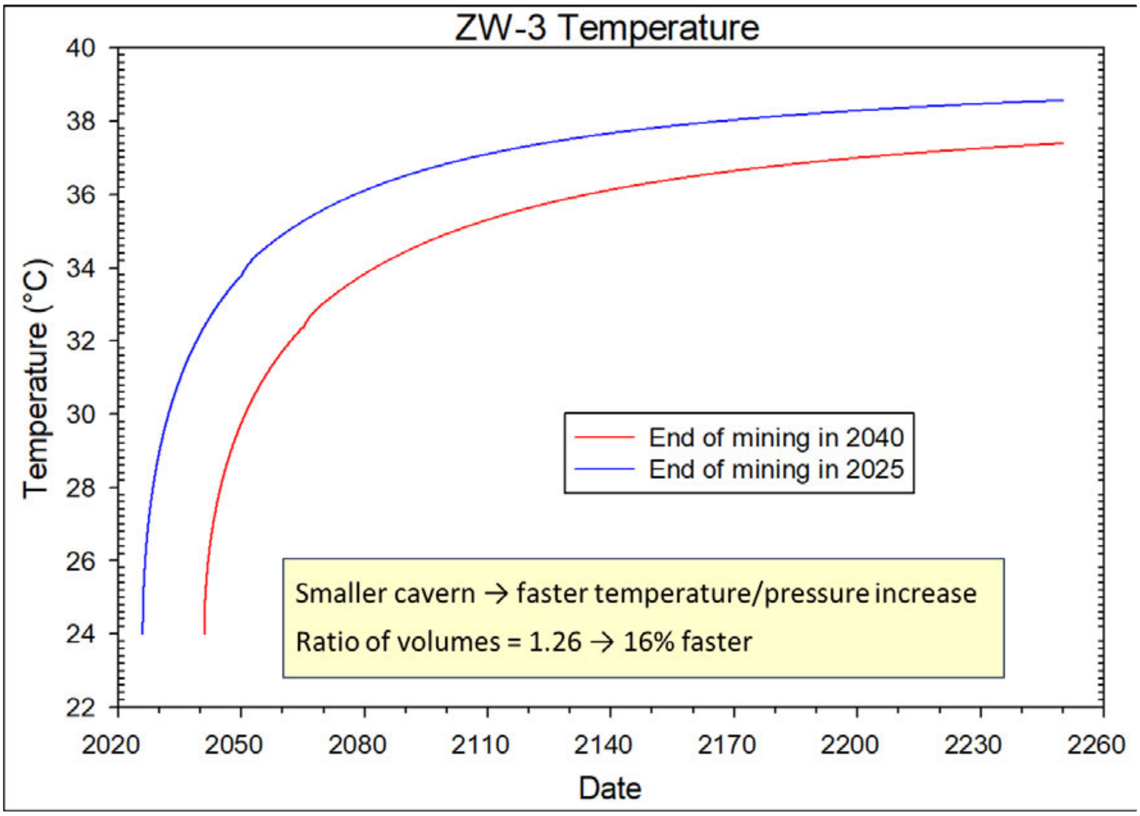

Figure 27. Comparison of temperature evolutions in the cavern depending on whether mining stops in 2025 or 2040.

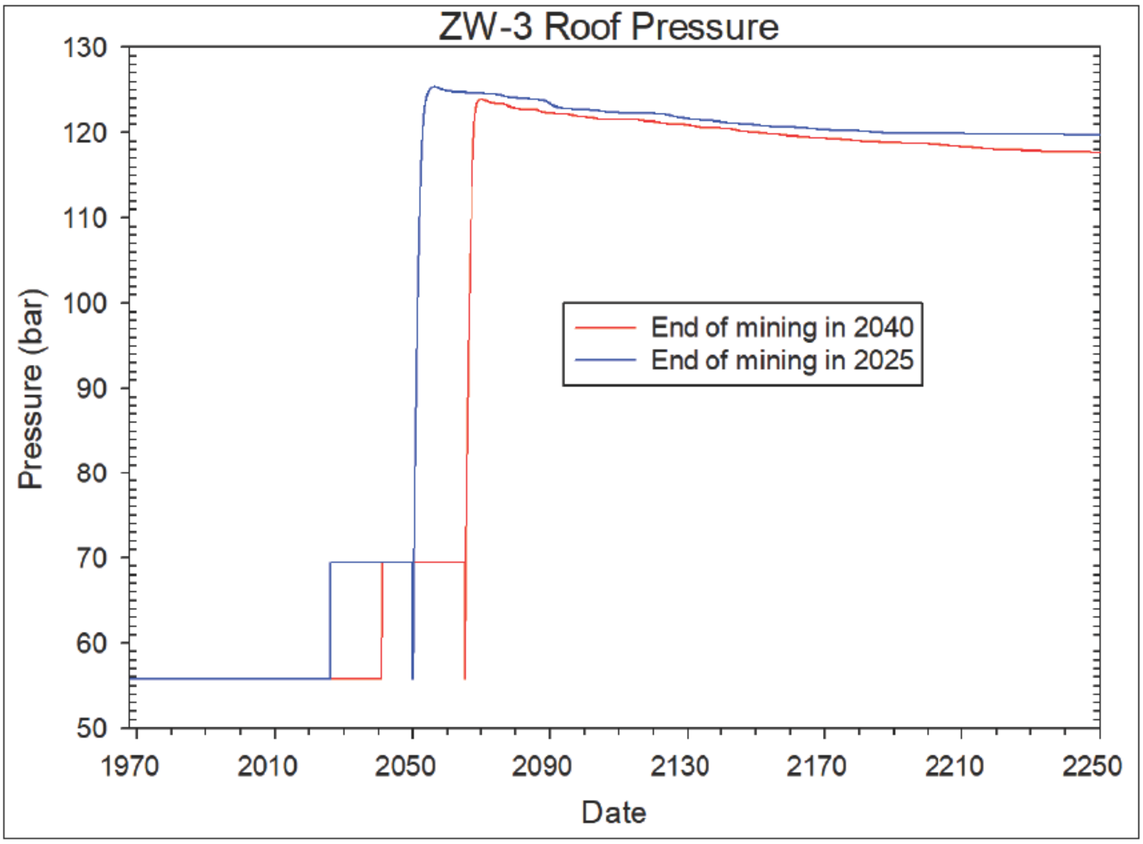

Figure 28. Comparison of pressure evolutions in the cavern depending on whether mining stops in 2025 or 2040.

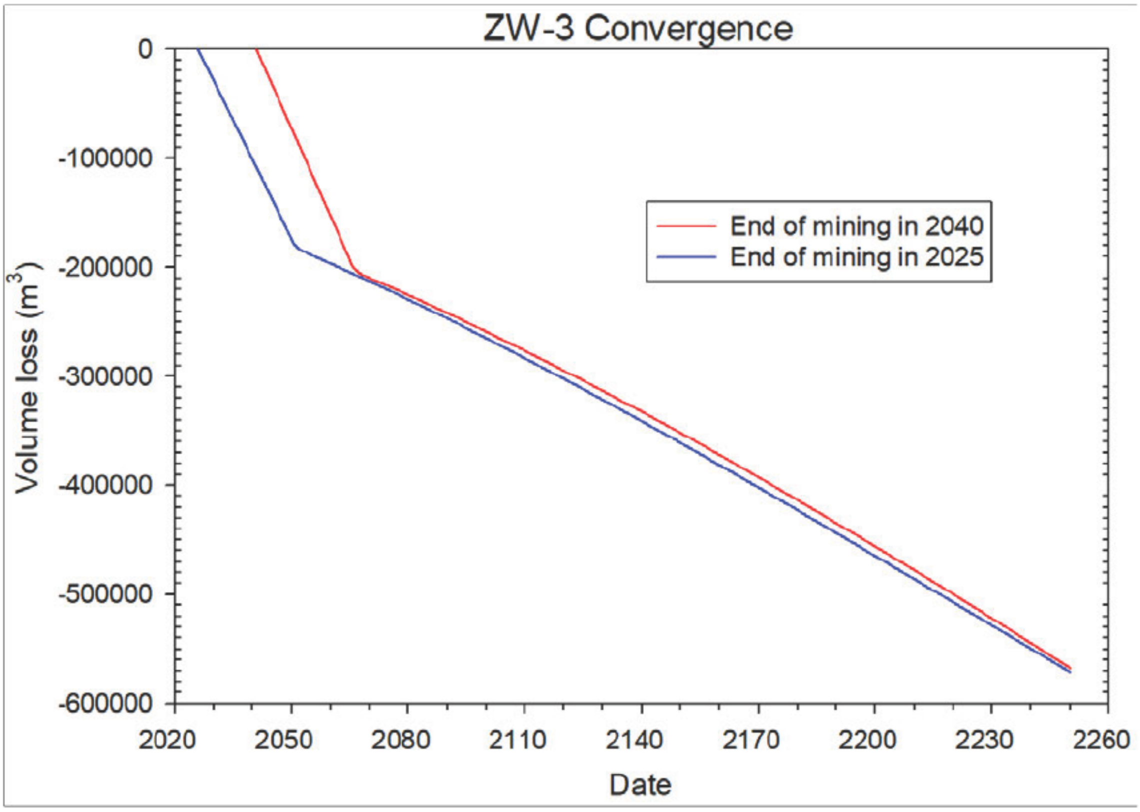

Figure 29. Comparison of the cavern convergence depending on whether mining stops in 2025 or 2040.

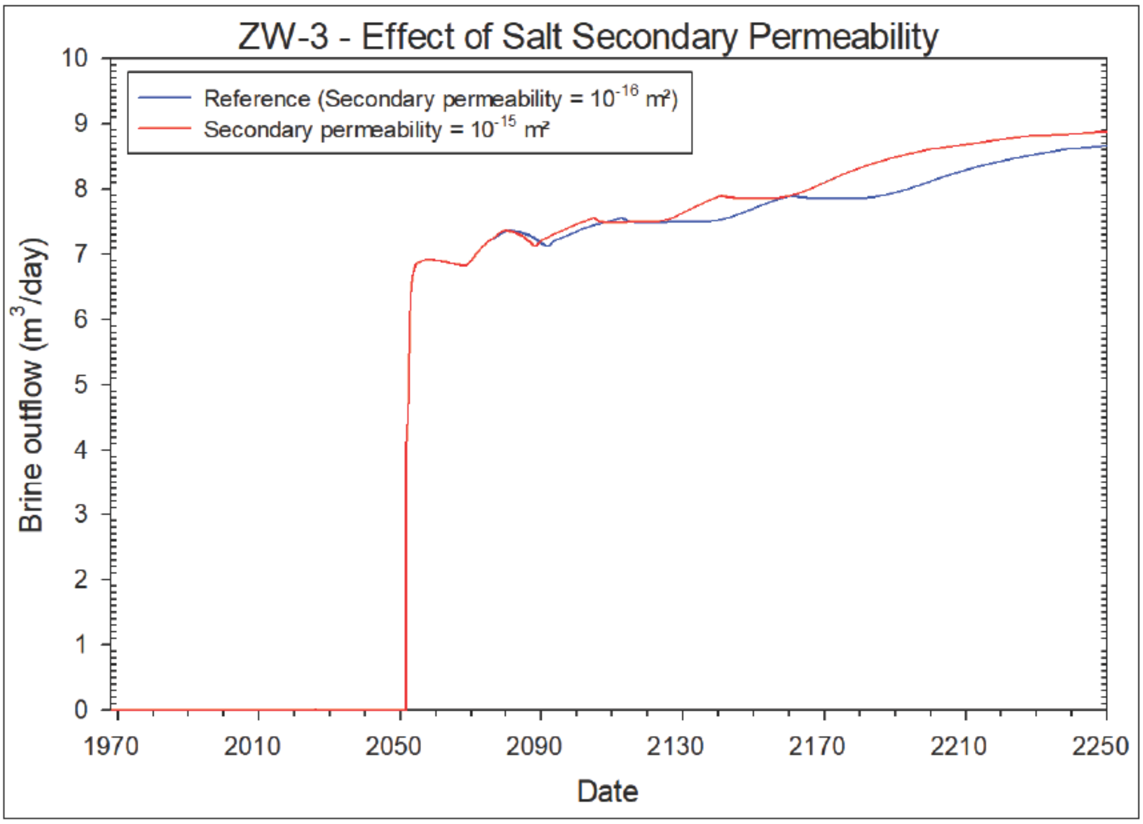

Figure 30. Comparison of the permeation rate depending on whether mining stops in 2025 or 2040.

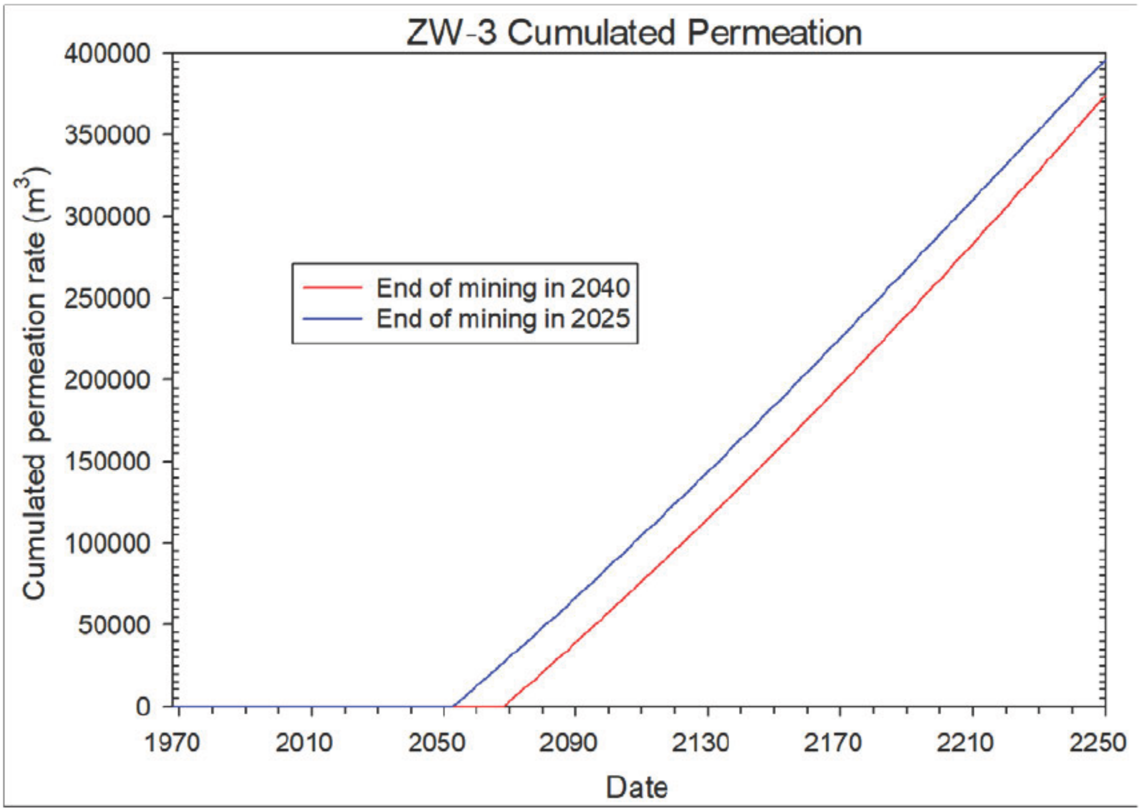

Figure 31. Comparison of the cumulated permeation depending on whether mining stops in 2025 or 2040.

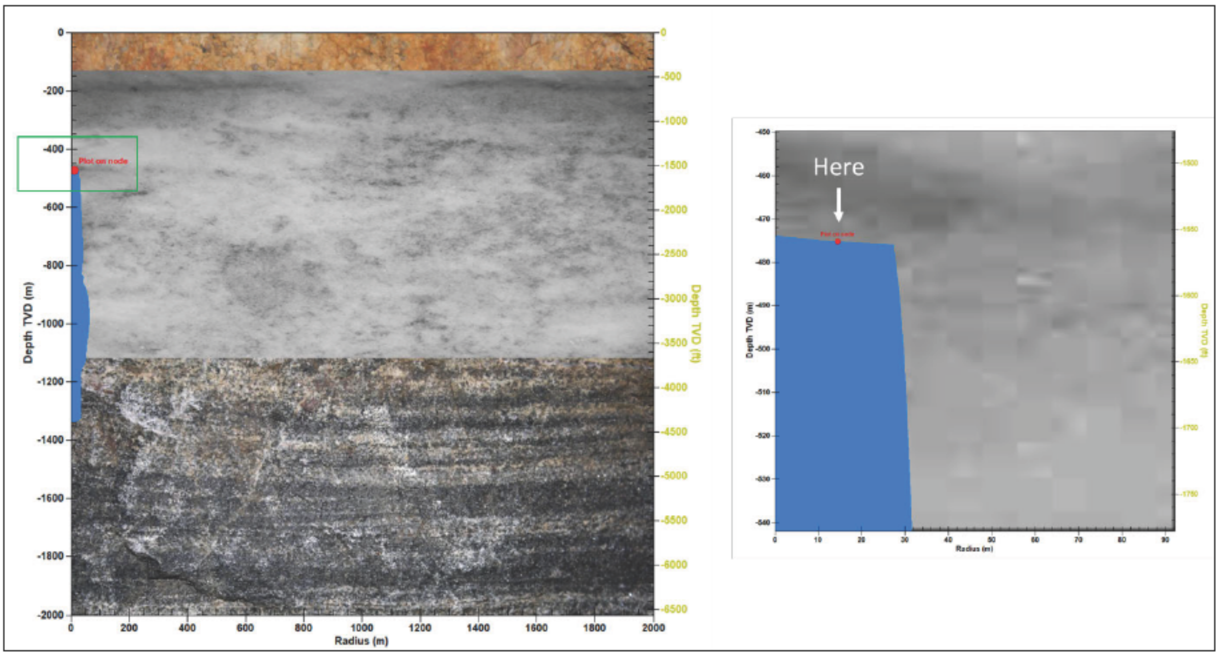

Figure 32. Point selected in the cavern roof.

Figure 33 shows the evolution of the stress state at a representative node on the wall in the cavern roof (Figure 32). This node is representative because it is located in a sensitive area where there is a risk of dilatation or even fracture. We can see that the state of the stress follows a fairly complex path, and that dilation appears at the beginning and end of the waiting period when assuming the very conservative DeVries criterion. This is due to the fact that a rapid change in pressure in the cavern creates additional elastic stresses which is superimposed on the initial stress field. Dilation does not imply a fracture growing out of the near-cavern area, as the brine pressure is relatively low at that moment. After abandonment, the mean stress tends to increase due to cavern convergence and the shear stress tends to decrease due to stress relaxation, which removes the risk of dilation occurring.

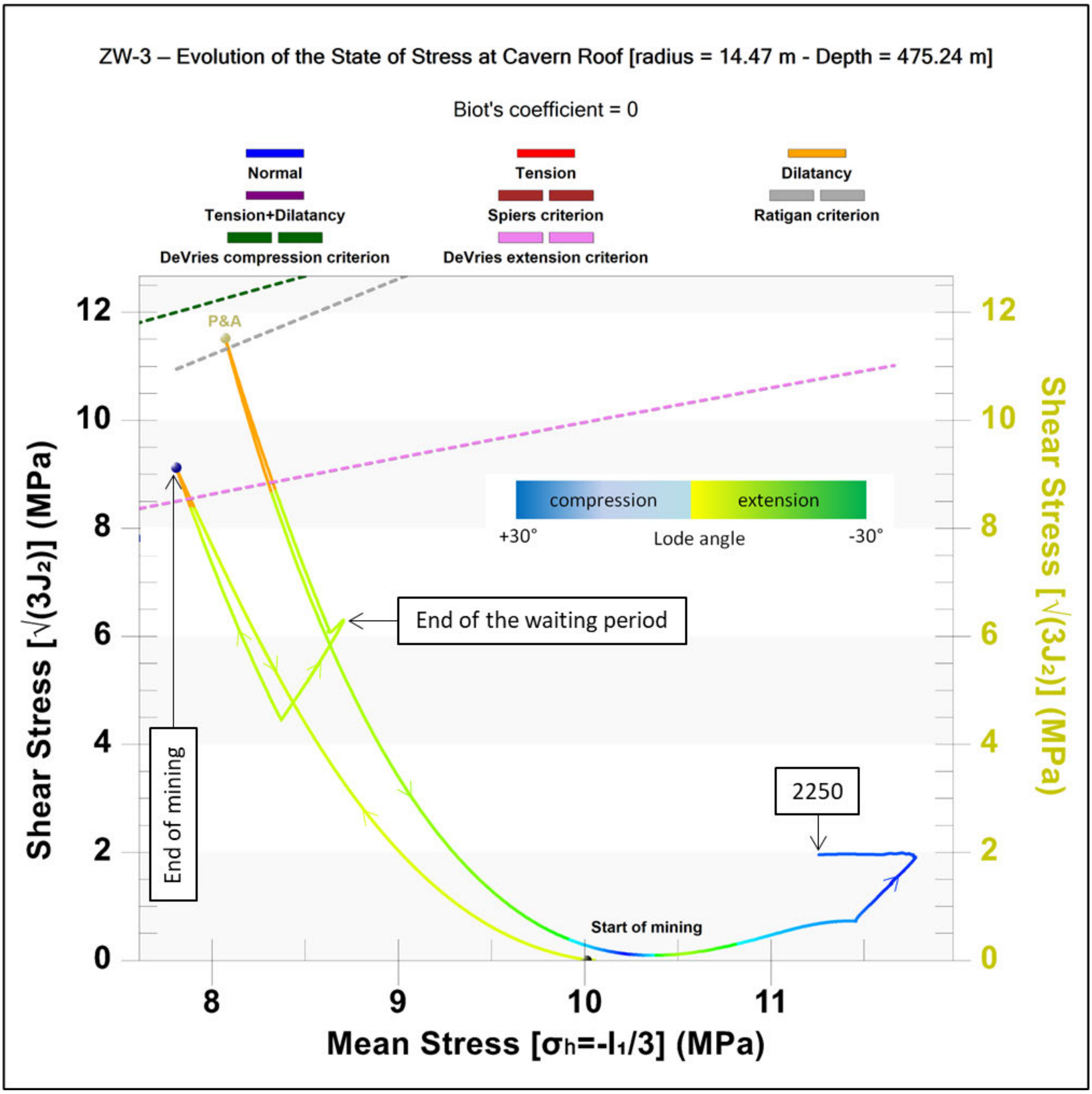

Figure 33. Evolution of the state of stress at the cavern roof.

Figure 34 shows a comparison of stress paths in the two cases. The risk of dilatancy occurring is slightly lower in the 2040 case because, although the additional elastic stresses are the same at the time of decompression prior to abandonment, we start from a stress state where the mean stress and shear stress are lower.

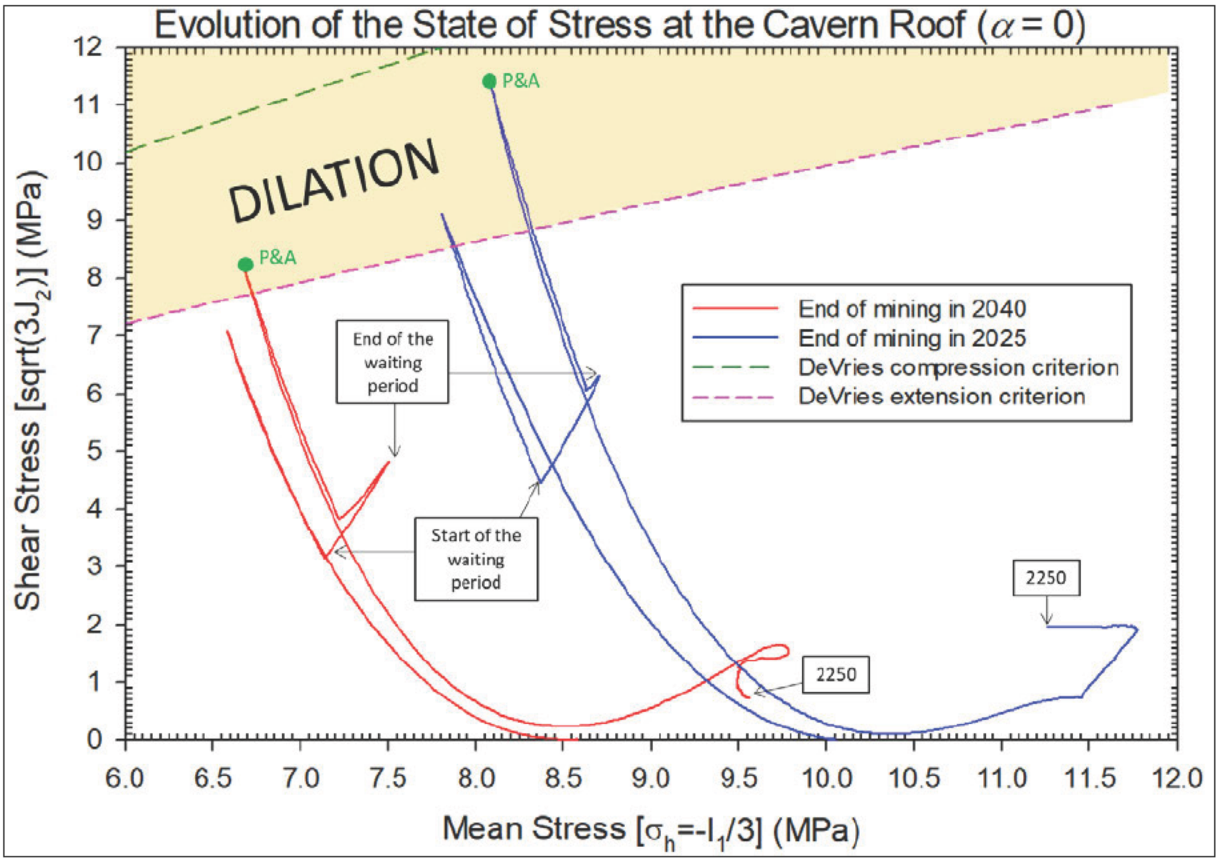

Figure 34. Comparison of stress paths in the two cases.

4.4 Conclusions

In the April 2024 report, we carried out a sensitivity study on the behaviour of the ZW-3 cavern because it is representative as it is the highest cavern of the group ZW-2 to ZW-9. These calculations were based on the planned end situation; i.e., end of mining of this cavern would end in 2040 (2035 in Nobian permit application). Where this document mentions 2040 to stay in line with the original CCC Zuidwending report (CCC, 2024), the same end shape and volume is meant as applied for 2035 in the Nobian extraction plan.

In terms of long-term evolution in pressure in the ZW-3 cavern, there is little difference between a scenario in which mining stops at the end of 2025 and the planned end volume (reached in 2040 in our simulations). In the 2040 case, the stresses have more time to redistribute, which slightly limits the risk of dilation occurring when cavern pressure increases relatively quickly just after the end of mining and just after the abandonment of the well (start and end of the waiting period). This difference is not very significant, especially as Nobian will be able to control the pressure rate during the waiting period.

In terms of the situation after abandonment, the likelihood of fracturing of the planned end shape of the cavern is also slightly lower compared to the end of mining in 2025 situation. However, given the compressibilities of the two caverns are in proportion to their volumes, in the event of the occurrence of a fracture that would partially decompress the cavern, it can be estimated that the volume expelled would be ~25% lower in the event of hydraulic fracturing after shutdown in 2025. This would result in a worst case volume of ~6400 m^3, a realistic case volume of ~2500 m^3, and an optimistic case volume of ~400 m^3 instead of ~8600 m^3, ~3300 m^3, and ~540 m^3 .

5 References

Baumann, T.S., Brouard, B., Popov, A. & Kottwitz, M.O. (2025). Beyond Axial Symmetry : The Critical Role of 3D Salt Dome Geometry in Cavern Closure and Subsidence Modeling. In The Mechanical Behavior of Salt XI (to be published).

Baumann, T.S, Kaus, B.J.P. & Popov, A. Over-pressured caverns and leakage mechanisms Part 3: Dome-scale analysis. https://kemprogramma.nl/file/download/28cef160-7ab4-41bc-87ca-698df3819931/15784005904.%20kem-17%20-%20over-pressured%20caverns%20and%20leakage%20mechanisms%20(final%20dome-scale,%204%20november%202019)%20(1).pdf

Bérest, P., Brouard, B., Feuga, B. & Karimi-Jafari, M. (2008). The 1873 collapse of the Saint-Maximilien panel at the Varangeville salt mine. International Journal of Rock Mechanics and Mining Sciences, 45(7), 1025–1043. https://doi.org/10.1016/j.ijrmms.2007.10.007

Bérest, P. (2016). Craters above salt caverns. Proc. SMRI Spring Meeting, Galveston, Texas.

Bérest, P., Sicsic, P. & Brouard, B. (2016). Thermomechanical effects of a depressurization in a CAES. Symp. Am. Rock Mech. Ass, Houston, Texas, ARMA 16-632.

Bérest, P. (2017). Cases, Causes and Classifications of Craters above Salt Caverns. Int. J. Rock Mech. Min. Sci. December 2017, 100, 318-329. https://doi.org/10.1016/j.ijrmms.2017.10.025

Bérest, P., Brouard, B., Karimi-Jafari, M. & Réveillère, A. (2020). Maximum admissible pressure in salt caverns used for brine production and hydrocarbon storage. Oil Gas Sci. Technol. – Rev. IFP Energies nouvelles 75, 76. https://doi.org/10.2516/ogst/2020068

CCC (2019). KEM-17 Over-pressured salt solution mining caverns and possible leakage mechanisms, https://kemprogramma.nl/blog/view/8357de0c-481d-4893-8ac1-4b2d1bc93aff/kem-17-over-pressured-salt-solution-mining-caverns-and-possible-leakage-mechanisms-finished

CCC (April 2024). Abandonment of solution mining cavern field Zuidwending, The Netherlands. Report for Nobian and Gasunie, 242 pages.

Debois, G., Urai, J.L., Schmatz, J., de Bresser, H. & Zavada, P. (2012). The distribution of fluids in natural rock salt to understand deformation mechanisms. In: Proc. Mechanical Behaviour of Salt VII

Denzau, H., Costinescu & Boor (1994). Konsortium "Druckaufbautest". Druckaufbautest in der Kaverne Etzel K102, Seismoakutische Überwachung. Report (in German).

DeVries, K.L. (2006). Geomechanical Analyses to Determine the Onset of Dilation Around Natural Gas Storage Caverns in Bedded Salt, in: Proceedings. Presented at the SMRI Spring Meeting 2006, SMRI, Brussels, Belgium, pp. 132–148.

DeVries K., Johnson C., Walega E. & Hladysz J. (2022). Correlation of Chemical, Mineralogic, and Physical Characteristics of Domal and Bedded Salt to Deformation and Strength Properties. SMRI Research Report RR2022-2, 242 pages.

Djizanne, H., Bérest, P. & Brouard, B. (2012). Tensile Effective Stresses in Hydrocarbon Storage Caverns. Proc. SMRI Fall Meeting, Bremen, Germany.

Fokker, P. & Smit A.J. (2024). State of the art cavern abandonment at Nedmag. Proceedings in Salt Cavern uses and abandonment: Bridging the technical and social perspectives. Salt Cavern Workshop 15 & 16 October 2024, Utrecht.

Ford, S. R., & D. S. Dreger (2020). Pre-Sinkhole Seismicity at the Napoleonville Salt Dome: Implications for Local Seismic Monitoring of Underground Caverns, Seismol. Res. Lett. 91, 1672–1678, doi: 10.1785/ 0220190224.

Houben, M., ten Hove, A., Peach, C.J. & Spiers, C.J. (2013). Crack healing in rocksalt via diffusion in adsorbed aqueous films: Microphysical modelling versus experiments, Physics and Chemistry of the Earth, Parts A/B/C, Volume 64, Pages 95-104.

Karimi-Jafari, M., Berest, P. & Brouard, B. (2008). Some Aspects of the Transient Behavior of Salt Caverns. Proc. SMRI Fall Meeting, Rapid City, South Dakota.

Karimi-Jafari, M., Berest, P. & Brouard, B. (2008). Subsidence, sinkholes, and craters above salt caverns. Proc. SMRI Spring Meeting, Porto, Portugal.

KEM-17 studies (2019). https://www.sodm.nl/documenten/rapporten/2020/02/11/onderzoek-langetermijnrisicos-afsluiten-zoutcavernes

Jaeger, J. C., Cook, N. G., & Zimmerman, R. Fundamentals of rock mechanics, 2007. Pub. by John Wiley & Sons.

Popp, T., Wiedemann, M., Kansy, A. & Pusch, G. (2007). Gas transport in dry rock salt – implications from laboratory investigations and field studies, in: Proceedings. Presented at the 6th Conference Mechanical Behaviour of Salt, Taylor & Francis, pp. 17–26. https://doi.org/10.1201/9781315106502-3

Popp, T., Minkley, W., Salzer, O. & Schulze, K. (2012). Gas transport properties of rock salt—synoptic view, in: Proceedings. Presented at the 7th Conference Mechanical Behaviour of Salt, Taylor & Francis, pp. 143–153.

Rokahr, R., Staudtmeister, K. & Zander-Schiebenhöfer, D. (1998). Rock Mechanical Determination of the Maximum Internal Pressure for Gas Storage Caverns in Rock Salt. Proc. SMRI Fall Meeting, 4-7 October 1998, Roma, Italy.Rokahr, R.B., Hauck, R., Staudtmeister, K. & Zander-Schiebenhöfer, D. (2002). High Pressure Cavern Analysis. SMRI Research Report 2002.

Schoenherr, J., Urai, J.L., Kukla, P.A., Littke, R., Schleder, Z., Larroque, J.-M., Newall, M.J., Al-Abry, N., Al-Siyabi, H.A. & Rawahi, Z. (2007). Limits to the sealing capacity of rock salt: A case study of the infra-Cambrian ara salt from the south Oman salt basin. AAPG Bulletin 91, 1541–1557.

Schmatz, J., Wellmann, E., Jian, M., Klaver, J., Bakker, R.B., den Hartogh, M., Hermann, J., Rölke, C. & Naumann, D. (2024). Microstructural Investigation of Heterogeneous Rock Salt Permeation: Unraveling the influence of Anhydrite and MegaGrain content on Fluid Transport. Proc. SMRI Spring Meeting, Krakow, Poland, 205-223.

Staudtmeister, K. & Rokahr, R.B. (1994). Pressure Build-Up Test in the Etzel K 102 Cavern. SMRI Research Report 98-5, 176 pages.

Stormont, J.C. (2001). Evaluation of Salt Permeability Tests. SMRI Research Report.

Urai, J., Schmatz, J. & Klaver, J. (2019). Over-pressured salt solution mining caverns and leakage mechanisms. KEM-17 Report. https://www.sodm.nl/binaries/staatstoezicht-op-de-mijnen/documenten/rapporten/2020/02/11/onderzoek-langetermijnrisicos-afsluiten-zoutcavernes/KEM-17+Micro-scale.pdf

White, A.J., Traugott, M.O. & Swarbrick, R.E. (2002). The use of, M.O., and Swarbrick, R.E., 2002. The use of M.O., and Swarbrick, R.E., 2002. The use of leak-off tests as means of predicting minimum in situ stress. Pet. Geosci., 189–193.

Zijp, M.H.A.A. , Huijgen, M.A. , Wilpshaar, M., Bouroullec, R. & ter Heege, J.H. (2018). Stringers in Salt as a Drilling Risk. Report, TNO2018 R10975.

APPENDIX

A. Importance of the transient component of dislocation creep law

In all the numerical simulations carried out to date, we have always considered only the stationary part of the creep dislocation law, in this case the Norton-Hoff law, based on the assumption that the transient part of the dislocation creep mechanism is not of major importance in the context of cavern abandonment. In order to verify that assumption, we simulated the abandonment of the ZW-3 cavern in 2050 (after end of mining in 2025) using the Munson-Dawson law (Figure 35), which incorporates the Norton-Hoff law for the stationary part and also a transient component. The set of parameters used for the transient part corresponds to the Avery Island dome salt, which is very well documented and on which Munson-Dawson calibrated their law, the stationary part being that calibrated for Zuidwending (Figure 36).

$$\dot{\varepsilon}_{ij}^{vp} = \frac{\partial \sigma}{\partial \sigma_{ij}} F \dot{\varepsilon}_{ss} \qquad \begin{cases} F = e^{\Delta\left(1-\varsigma/\varepsilon_t^*\right)^2} & \text{when } \varsigma \le \varepsilon_t^* \\ F = e^{-\delta\left(1-\varsigma/\varepsilon_t^*\right)^2} & \text{when } \varsigma \ge \varepsilon_t^* \end{cases}$$

$$\dot{\varsigma} = \left(F-1\right)\dot{\varepsilon}_{ss} \qquad \dot{\varepsilon}_{ss} = A\exp\left(-Q/RT\right)\sigma^n$$

$$\sigma = \sqrt{3J_2} \qquad J_2 = \frac{1}{2} s_{ij} s_{ij}$$

$$\varepsilon_t^* = K_0 e^{cT}\left(\sigma/\mu\right)^m$$

$$\mu = \frac{E}{2\left(1+\nu\right)} \quad \text{and} \quad \Delta = \alpha_w + \beta_w Log_{10}\left(\sigma/\mu\right)$$

Figure 35. Formulation of the Munson-Dawson law for dislocation creep.

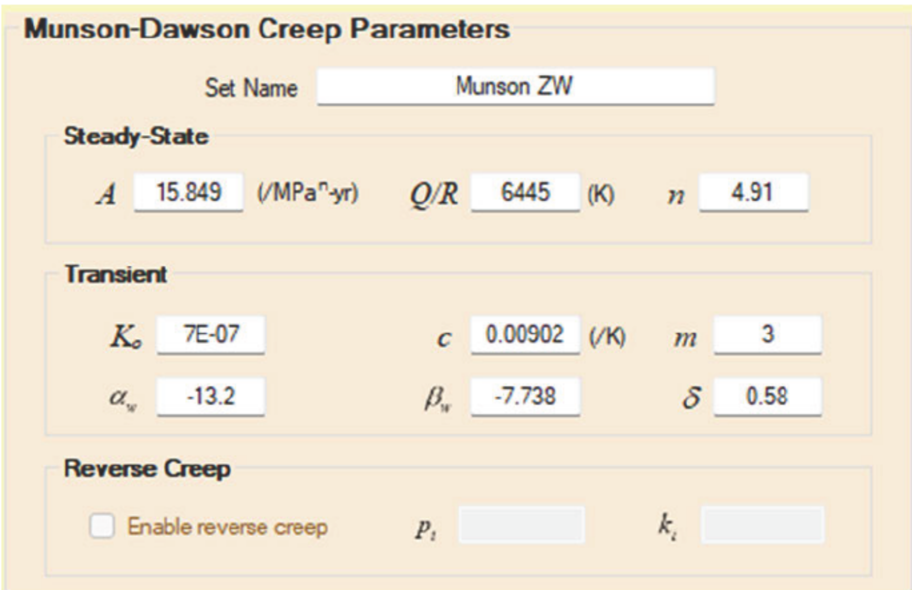

Figure 36. Set of parameters considered for the simulation.

Figure 37 shows the evolution of the pressure at the roof of the ZW-3 cavern, assuming that it is abandoned in 2050 (end of mining in 2025). It can be seen that the difference between the two laws is very small, in particular it does not modify the maximum pressure reached after abandonment.

In conclusion, this calculation confirms that for abandonment calculations, the stationary Norton-Hoff law is sufficient for the dislocation creep mechanism.

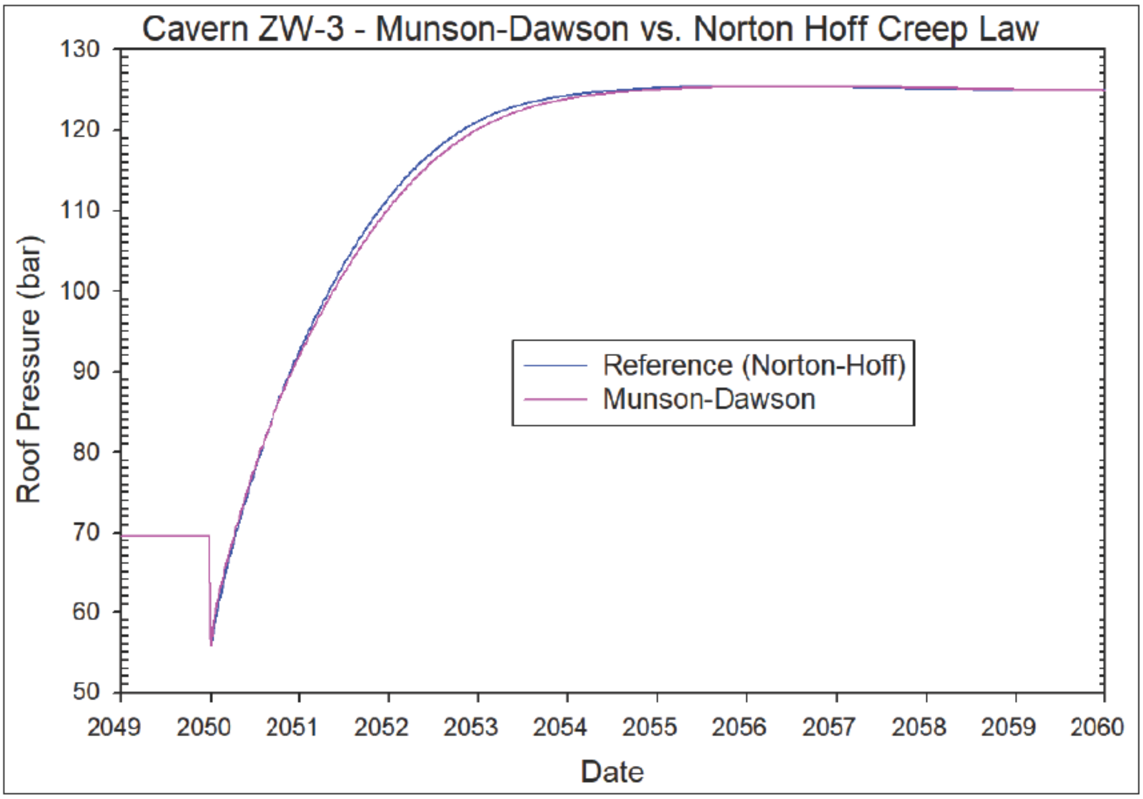

Figure 37. ZW-3 - Pressure evolution at cavern roof. Effect of the transient component of the dislocation creep law.

B. Case of higher secondary permeability

For most of the numerical simulations, a secondary salt permeability of 10^{-16} m^2 was assumed (Figure 39). This value could not be accurately determined by laboratory tests performed by IfG. In the tests carried out by the Ecole Polytechnique for the SMRI (Rokahr et al., 2002), it was possible to calculate permeabilities greater than 10^{-16} m^2 (Stormont, 2001), which is why it seemed interesting to compare the pressure evolution in the ZW-3 cavern in the case of a secondary permeability 10 times greater, i.e. 10^{-15} m^2. Larger field-scale tests or even Etzel-like abandonment tests are required to better constrain permeation behaviour.

Figure 40 shows the evolution of the pressure at the roof of the ZW-3 cavern in the two cases. It can be seen that a larger secondary permeability of the salt has the effect of reducing the maximum pressure reached in the cavern after abandonment. The maximum pressure gradient decreases from 0.264 bar/m (10^{-16} m^2 case) to 0.242 bar/m (10^{-15} m^2 case).

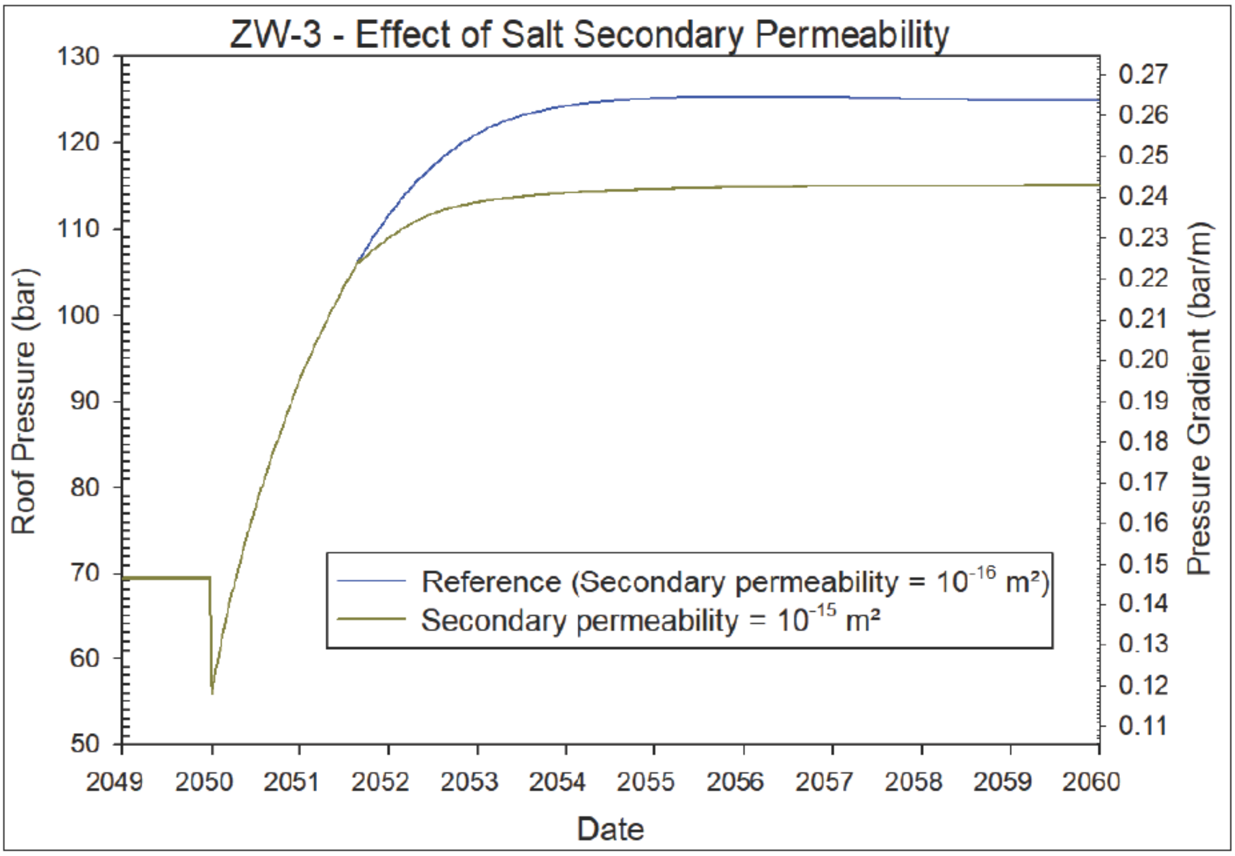

Figure 38. ZW-3 - Pressure evolution at cavern roof. Effect of secondary permeability.

Figure 40 and Figure 41 show the flowrate and cumulated volume of brine leaving the cavern due to permeation, respectively. Although the secondary permeability is 10 times greater, the stabilised permeation flowrate is larger by 40%, but less than 10 m^3/day in year 2250. It's a tiny flowrate when compared to the huge amount a salt in the cavern roof (> 2.5×10^8 m^3).

Figure 42 shows the permeability field at the end of the calculation (year 2250) in the case of a secondary permeability of 10^{-16} m^2 or 10^{-15} m^2. In the second case, the zone where permeability has increased is less wide and more concentrated above the roof of the cavern.

In conclusion, the effect of a higher secondary permeability is to reduce the maximum pressure reached by increasing the permeation flow, which remains small, by 40%.

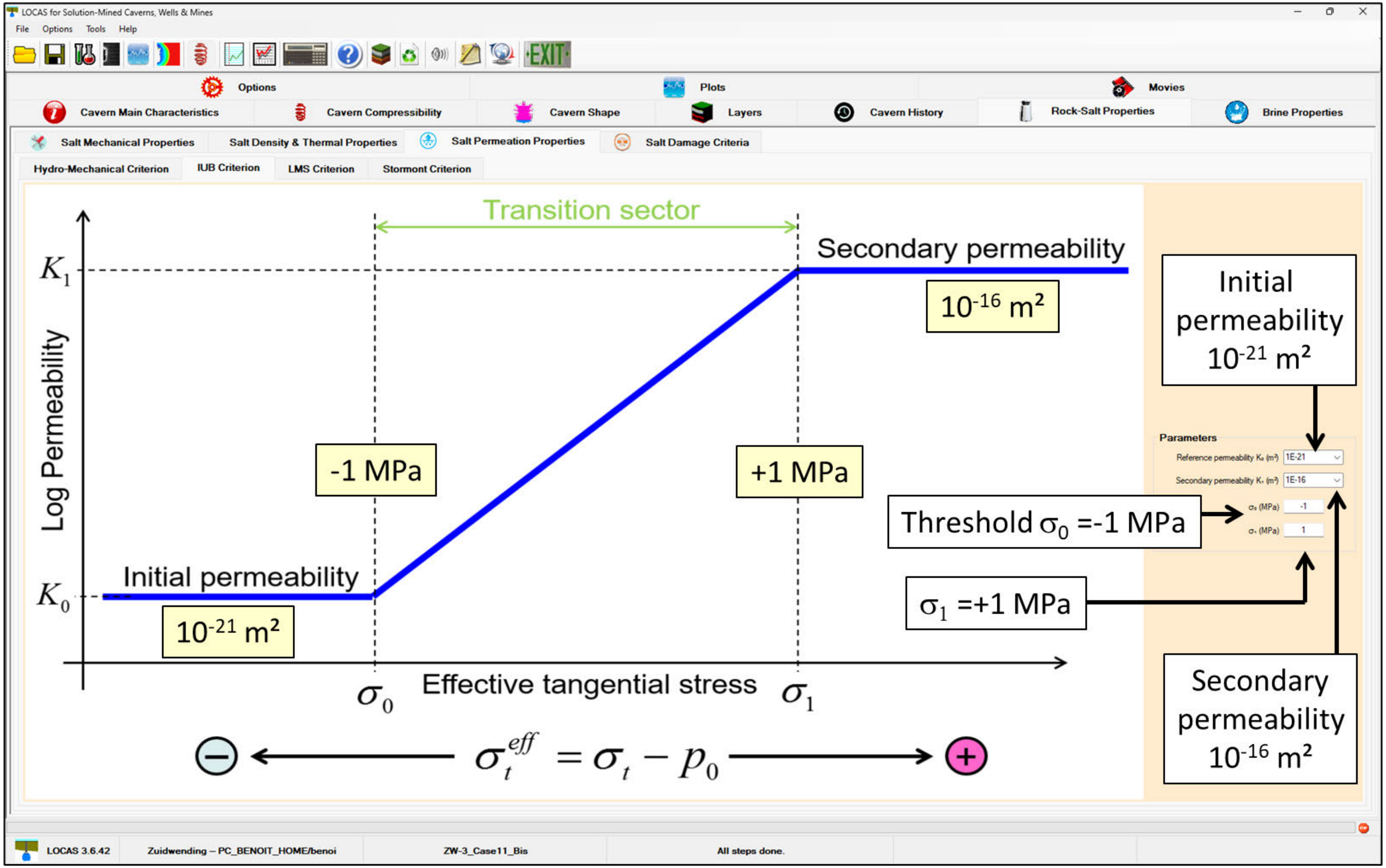

Figure 39. Parameters for the coupling between permeability and effective tangential stress in LOCAS.

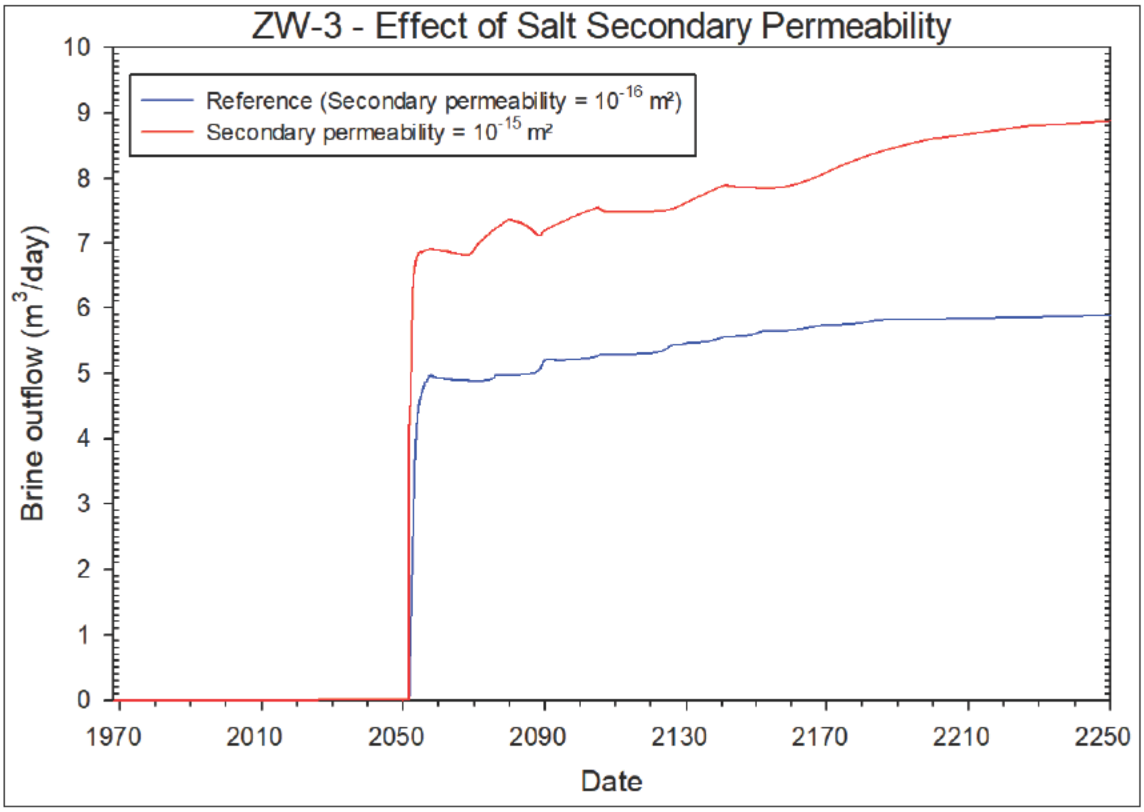

Figure 40. Brine outflow rate from cavern to overlying salt due to permeation after the abandonment of cavern ZW-3.

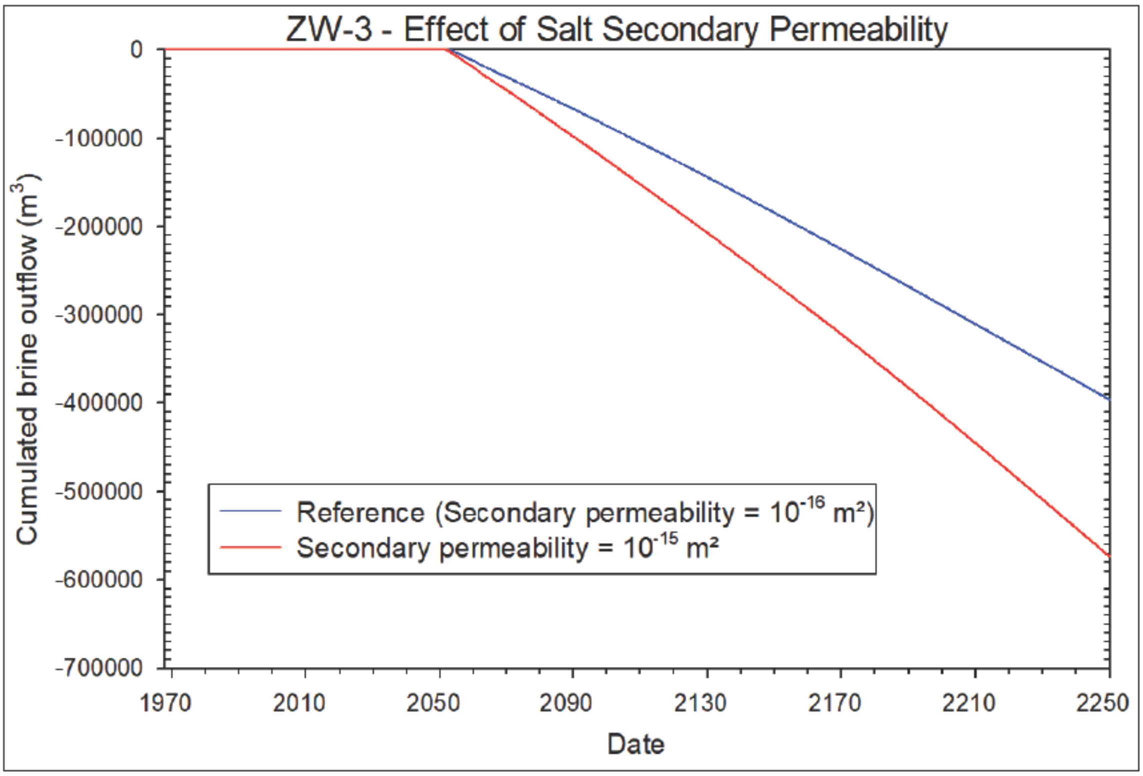

Figure 41. Cumulated brine outflow from cavern to overlying salt due to permeation after the abandonment of cavern ZW-3.

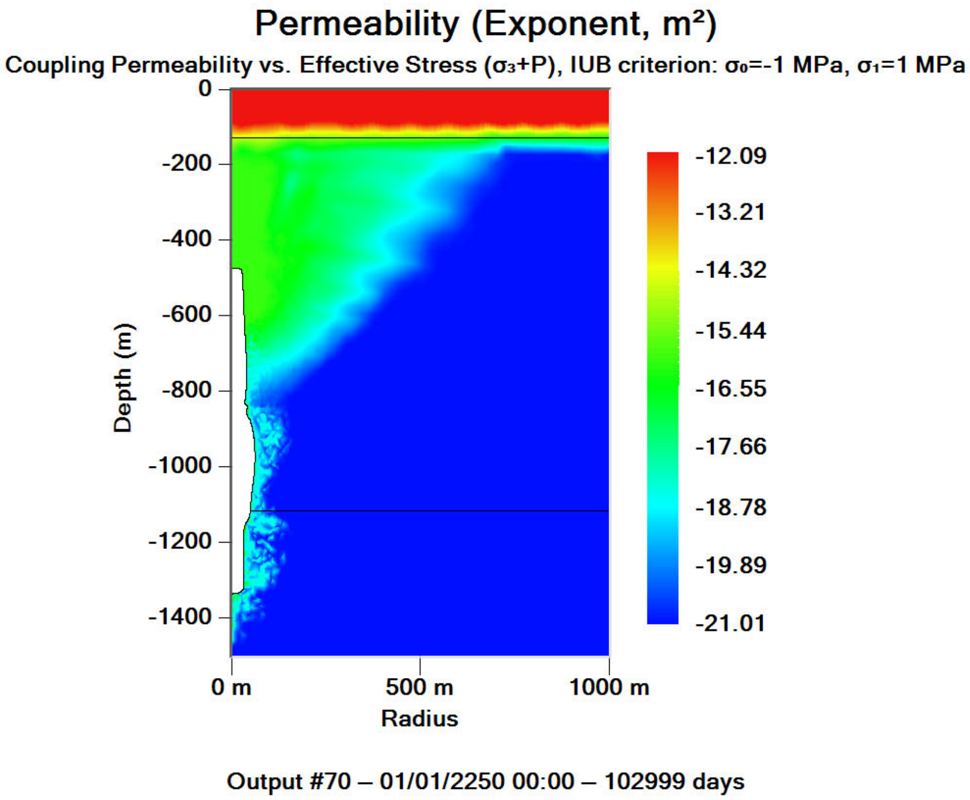

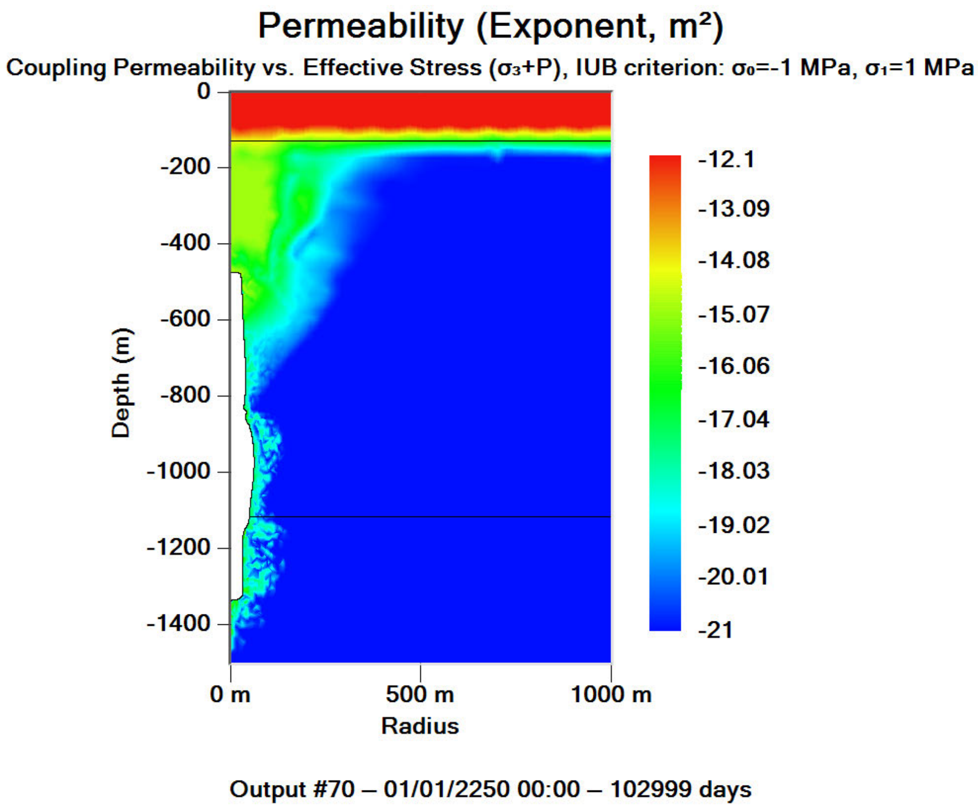

Figure 42. Permeability field at the end of the calculation in the case of a secondary permeability of 10^{-16} m^2 (top) or 10^{-15} m^2 (bottom).